LAPPEENRANTA UNIVERSITY OF TECHNOLOGY
School of Technology
Technomathematics and Technical Physics

Zaritovskiy Mikhail

RADAR CROSS-SECTION MEASUREMENT USING THE DOPPLER EFFECT

Examiners: Professor Erkki Lahderanta
Professor Lavrov A.P.

ABSTRACT

Lappeenranta University of Technology
School of Technology

Technomathematics and Technical Physics Radar cross-section measurement using the Dopler effect

2014

54 pages, 37 figures, 2 tables

Examiners: Professor Erkki Lahderanta
Professor Lavrov A.P.
Keywords: cross-section, effective scattering, Doppler effect, antenna, signal modeling, filtering.

Radar cross section measurement using conductive solid surfaces of different shape.

In this Master Thesis we discuss issues related to the measurement of the effective scattering surface, based on the Doppler Effect. Modeling of the detected signal was made. Narrowband signal filtering using low-frequency amplifier was observed. Parameters of the proposed horn antennas were studied; radar cross section charts for three different objects were received.

Contents

Symbols and abbreviations 4
Introduction 5
1. RCS MEASUREMENTS 6
1.1. RCS and RCS charts 6
1.2. Modeling for measuring the scattered waves 9
Electrodynamics modeling 10
1.3. Sources of parasitic scattering waves. Methods of dealing with them. 11
1.4. Methods for measuring the scattered waves. Doppler effect. 14
1.5. Variations in measurements of the scattered waves 17
2. DESCRIPTION OF LABORATORY EQUIPMENT 18
2.1. Laboratory-scale plant 18
2.2. Devices geometry and specifications. 21
2.3 Horn antenna transceivers 26
3. SIGNAL MODELING OF RF DETECTOR 29
3.1. Calculation of the phase change signal 29
3.3 Simulation of bandpass filtering of the signal from a detector 33
4. MEASUREMENTS 37
4.1. Registration of signals 37
4.2 Calibration of the system 39
4.3 Methods of Signal Processing 44
4.4. Comparison with previously published data 50
Conclusion 53
References 54

Symbols and abbreviations

RCS – radar cross-section

LF – low frequency

HF – high drequency

AM – amplitude modulation

RF – radio frequency

FFT – fast Fourier transform

DIP - dual In-line package

Introduction

Radio waves as any other natural waves in the same manner are reflected from an obstacle. Obstacle to the radio waves is any electrical or magnetic inhomogeneity of the medium parameters. Object will reflect electromagnetic energy if its conductivity, dielectric or magnetic permeability differ from the corresponding parameters of the environment. Electromagnetic fields of individual elementary currents in various points of a space are summed with different phase relations. Therefore the nature of the secondary radiation depends on the material from which the object is made, the shape and dimensions of the object, as well as the length of the incident wave and its polarization.

To determine the range of the radar station it is convenient to introduce some generalized parameter σ, which characterizes the scattering properties of the target, which does not depend on the parameters of the radar station. This parameter is called the radar cross section (RCS). RCS is studied in an academic discipline [1] and arouse a great interest. Therefore, it is advisable to familiarize students with it, and that was done in the lab, "Antennas and Microwave" in STU. There was prepared laboratory work "Study of electromagnetic wave scattering from conductive solids of different shape," as described in the manual [2].

As well, it is useful to pay the students' attention to the Doppler effect which is used in this Lab. Setup which was build to use this effect allows to fight with adverse reflected signals, which significantly improves the results of the study.

1. RCS MEASUREMENTS

1.1. RCS and RCS charts

Radar cross-section (RCS) describes the scattering properties of the target and does not depend on the parameters of the radar. Substituting the values of RCS into radar equation we can determine the range of the radar to this purpose.

Radar equation when receiving waves with the same polarization is:

$$P_{rec} = \left(\frac{P_{rad}\, G}{4\pi R^2}\right)\left(\frac{\sigma}{4\pi R^2}\right)S_{eff} \qquad (1.1)$$

where P_{rec} is received power; P_{rad} is radiated power; G is transmitting antenna gain; S_{eff} is effective area of the receiving antenna and σ is radar cross-section.

The right side of the equation has three factors. The first is a power flux density of the incident wave at the location of the target. Second factor is scattered power flux density at the location of the radar. Multiplying these two factors by the effective area of the antenna, we obtain the value of the power delivered to the receiver.

To determine the real purpose of the RCS, it is replaced by a dummy lens, which is positioned on the real target place and dissipates the energy uniformly in all directions, creating the same power density on a receiver in as the real target. If the RCS of the dummy lens is σ, then multiplying it by the incident power flux density of P_1, all the power falling on the lens is equal $P_1\sigma$. Then the power flux density at the site of the receiving antenna is equal to

$$P_2 = P_1\sigma/4\pi R^2 \qquad (1.2)$$

Hence, we usually write the expression that defines the value of the RCS in the following form:

$$\sigma = \lim_{R\to\infty} 4\pi R^2 \frac{P_2}{P_1} \qquad (1.3)$$

RCS depends on the shape and size of lens, material properties of the lens and of the operating wave length. As can be seen from the formula that determines the RCS, it also depends on the distance from the lens *R*, but if the distance becomes so large that the waves incident on the diffuser and the receiving antenna can be considered as flat, so RCS does not depend on the distance.

This expression is valid for the case where the transmitting and receiving antennas are combined or are in close proximity to each other. In the biradar case when the receiving and transmitting antennas are away from each other, the concept of RCS as well really. Radar equation becomes:

$$P_{rec} = \left(\frac{P_{rad}\, G}{4\pi {R_{rad}}^2}\right)\left(\frac{\sigma}{4\pi {R_{rec}}^2}\right) S_{eff} \qquad (1.4)$$

where R_{rad} is the distance from the lens to the transmitter on the transmitting station; R_{rec} is the distance from the lens to the receiving station.

RCS charts

Diagram showing the dependence of the RCS from the angle of incident waves is called the RCS diagram [1]. For the full knowledge of the characteristics of a lens diagram requires knowledge of the RCS in the entire field. Furthermore, the diagram is dependent on the polarization of the working length of the wave reflector so one may need a large number of diagrams. It is pretty expensive, so researches try to manage with less number of measurements. For some purposes it is interesting to get only a certain set of angles, and they can restrict with the measurements of RCS diagram. For axisymmetric bodies, which include cylindrical, conical body and other bodies of revolution, the RCS diagrams are also

bodies of revolution. Therefore it is sufficient to measure a single chart in the same plane for each polarization. Spatial RCS diagram is obtained by rotating the measurement chart around its axis of symmetry.

For complex bodies RCS diagrams are shot in azimuth angles for some angles of elevation. They are used to build diagrams of the spatial RCS in spherical coordinates or a cartographic diagramm.

As a result of laboratory measurements RCS static diagrams are obtained. They show the importance that the RCS conforms to this angle of incidence of the waves on the target. If you know the time variation of the position of the target and its range, then using a static diagram, you can build a dynamic diagramm - time dependence of the signal received by the station. In most cases the movement of the target relative to the radar is random and dynamic chart is a subject for statistical processing.

Scatterplots

Scattering matrix (SM) elements are functions of the angle at which the incident waves go to the lens, as well as the angle between the normals of the incident and scattered waves. We have complete information when we know the charts of all elements of SM, for all angles of incidence of the waves on the diffuser and for all angles between the directions of radiation and reception.

Consider a spherical coordinate system (R, θ, φ) with the origin at the center of the lens. We assume that the transmitter is fixed and is always at ($R_{rad}, \pi / 2, 0$). Receiving point can be changed and determined by coordinates ($R_{rec}, \theta_0, \varphi_0$). Finally, the main axis of the lens $O' - O''$ can be rotated around the axis z, forming an angle γ with the x axis. The following types of diagrams cause the practical interest:

1. Scattering diagram determines the nature of the scattered field around the lens with a fixed position and direction of the lens exposure. Scattering diagram is measured by moving the receiving installation around lens at a fixed distance from the foot ($R_{rec} = const, \theta = var, \varphi = var, \gamma = const$).

2. Backscattering diagram shows the dependence of the scattered field from the position of the lens combined with the receiving and transmitting units (single case) or in close proximity to one another (called kvasi-single position case). . Backscattering diagram is measured by the rotation around the axis of the diffuser ($R_{rec} = R_{rad} = const, \theta_{rec} \approx \frac{\pi}{2}, \varphi_{rec} = 0, v = var$)..

3. DIP scattering diagram which shows the dependence of the scattered field from the perspective of a lens as the distance between the receiving installation relative transmission (DIP-case). DIP scattering diagram is measured by the rotation around the z axis of a lens and the location of the receiving installation at ($R_{rec}, \theta_0, \varphi_0$). Usually in such measurements the distance is $R_{rec} = R_{rad}$ ($R_{rec} = R_{rad} = const, \theta_{rec} = \theta_0, \varphi_{rec} = \varphi_0, \gamma = var$). For dimensional diagram transmission installation is placed successively in several points of the plane φ = 0 for different values θ_{rad}. The magnitude R_{rad} is the same at all points. For each of the measured values θ_{rad} it makes DIP scattering diagram and it builds spatial backscatter diagram.

1.2. Modeling for measuring the scattered waves

Measurement of scattering properties of different radar targets in real conditions is costly and time consuming process. Simulation allows to get the information you need with minimal funds and in the short term.

Physical modeling is using any wave processes in which the scattering phenomenon is similar to the scattering of radio waves. For example, ultrasonic and light waves.

RCS measurement methods and elements of the scattering matrix (SM) measurements are divided into natural objects measurements and models measurement. In the measurement of natural objects, dynamic charts prepared RCS and SM. It is quite difficult to get a static diagram from that measurements, i.e. RCS and elements of SM are depending on the angle of incidence waves because it is difficult to determine accurately the targets' laws of motion. Therefore, measurements in real conditions are limited by measuring dynamic charts and statistical definition of reflection.

Under laboratory conditions in landfills or in an anechoic chamber it is often measured RCS of targets or layouts in a full size. Measured objects are in uniform rotation using little reflection rotators.

The most commonly accepted method is direct simulation based on the terms of the electrodynamic similarity. Also indirect modeling techniques are widespread when coherent or incoherent light and sound waves are used. For example, a simulation method using sound waves in the water bath is easy to visually observe the pattern of wave propagation around the goal, but the quality values are difficult to obtain. Furthermore, the wave in the water bath are more similar in their properties to radio waves in the waveguide than in free space.

Electrodynamics modeling

Modeling in electrodynamic systems is used since the beginning of the twentieth century. This possibility was substantiated by Abraham [3]. Currently, this is the main method for determining the RCS and SM elements of various

bodies in a microwave laboratory. For a quasi-wave measuring, distance must satisfy the condition

$$R \geq k\frac{L^2}{\lambda} \qquad (1.5)$$

or, when expressed L in the wavelengths, i.e. enter $L_\lambda = L/\lambda$, then

$$R \geq k\lambda L_\lambda^2 \qquad (1.6)$$

As can be seen, when $L_\lambda = const$, required distance is directly proportional to the wavelength and decreases in modeling as many times as shorter the wavelength. By measuring the models on the waves, many times shorter than the operation, it is possible to significantly reduce the distance to the measured sample.

Theoretically, it is possible to build a model that will display the configuration of the field near the object to be measured in relative units, as well as absolute levels of power. Then it is possible to measure the electromagnetic properties of the system, including the intensities of the incident and reflected fields. But the existence of such a model is very complex, so in a microwave range in practice only the relative simulation is used, when only field configuration is modeled. To obtain the absolute values of the field strengths or capacities it is necessary to use indirect methods of modeling.

Ability to create an electrodynamics system is based on the linearity of Maxwell's equations, so that nonlinear medium should be excluded from consideration. Electrodynamics simulation terms are valid only for systems with linear media, and they can be both homogeneous and heterogeneous.

1.3. Sources of parasitic scattering waves. Methods of dealing with them.

The primary task the researcher faces during scattering diagrams measurement is the need to create a space in which the object to be measured is set, with such field distribution, which is close to a quasi-wave field. Appropriate distance between the target and measuring assembly is selected or collimating devices are used.

Near the working volume there can be various items that scattered the wave. Scattered waves distort the field in the working volume and lead to errors in the measurements. Suppression of these emissions is a very important task, which is often impossible to be solved completely, but it is a necessary task to bring them up to a minimum value.

Support on which the measured object is fixed, is one of the main sources of scattering. In landfills it can be the surface of the soil, buildings, trees and other objects as well.

Modern measuring units are placed in anechoic chambers, the room in which the necessary actions are taken to suppress scattering from the walls. Anechoic chamber is usually made of rectangular section or horn shape, ranging in size from a few meters to several dozens of meters. Basically, shielded anechoic chambers are made with a damping factor of 80-100 dB and above.

Generally, the larger the size and the higher the quality of radar absorbing materials, the better the anechoic chamber. The sectional shape also affects the quality of an anechoic chamber. Measurements using them are more comfortable, efficient and accurate than in landfills.

Radio-absorbing materials

To suppress reflections from the walls, anechoic chambers are covered with special absorbing materials. The main requirement for materials is the low reflectance value in a wide range of angles - from 0^o to $80 - 85^o$. Also small

reflectance in a wide wavelength range is required. The requirements for the mechanical properties of the materials are sufficiently low, except the material that is coming for manufacturing floor.

The material is made of hard or soft foam-filled frame, well absorbing radio waves. To ensure low reflection of the material, density on its surface should be close to the density of the air. The density and concentration of absorber material increases with depth, and are chosen so that also the radio waves can be absorbed. Smooth change of electrical parameters with depth ensures there is no partial reflections within the material.

Thus, for the construction of anechoic chambers, radioabsorbing materials are used. They work in the centimeter and decimeter waves. These materials are significantly worse for meter waves. Radar absorbing materials are made with black surface. They are also able to absorb infrared light waves and radiation.

Support for the measured objects

This question is very important in engineering measurements of radar targets. Supports are used for fastening the measured object within the working volume, its rotation for measuring diagrams. The main task is to reduce the magnitude of the scattered signal from the support while retaining its mechanical rigidity.

For field installations where the weight of measured objects is large, supports are made of metal poles covered with radio absorbed materials that allows you to get the necessary minimum of the scattered signal. Just the magnitude of the scattered signal affects the correct selection of the angle of inclination of the mast.

For smaller size and weight objects, there are two common types of supports: foam support or nylon filaments. For the manufacture of columns of the low density foam is used with a dielectric constant $\varepsilon = 1.03 - 1.1$. It is known that

is the coefficient of reflection of radio waves is smaller, less different is between the permittivity of the material from the dielectric constant of air, that is equal to unity. Scattered signal decreases if shaping the support as a cylinder. If the diameter of the cylinder may be made equal to several wavelengths, the scattered signal can be significantly reduced. When operating at the same wavelength, the diameter of the cylinder may be selected so that the scattered signal is reduced by 30 - 40 dB.

1.4. Methods for measuring the scattered waves. Doppler effect.

Designing any type of measurement setup it is necessary to determine its "potential energy" and dynamic range.

Potential energy of the installation is the ratio of the radiated power of the transmitter to the receiver sensitivity. Necessary potential energy installation depends on various factors, the main ones are the size and shape of the measured body and the required accuracy.

To measure the scattered fields, there are many plants that have their own advantages and disadvantages.

Measurement setup with a CW

Measurement setup with continuous radiation has an advantage over other types of setups, that measurements are made in almost monochromatic vibrations. Because of this, it is easy to compare the experimental and theoretical diagrams, which are usually calculated for monochromatic waves. Such installations are simple, relatively cheap and reliable in operation. An essential element of the installation is the compensation path intended to compensate reflections from the support and other parasitic scatterers. However, usage of compensation for background suppression imposes certain requirements on the stability of the

oscillator frequency and consistency double the distance from the transmitter to the scatterer.

Measurement setup with frequency modulation (FM)

Installations with a frequency modulation allow selection of reflecting objects in range, which reduces spurious signals from the most harmful reflectors. The measuring apparatus uses an FM signal modulated in frequency. The most common installations work with frequency changing in a linear and sinusoidal laws.

To isolate the signal reflected from an object on a background of interfering scattering surrounding objects we can use the change in frequency due to motion of the source of electromagnetic radiation.

It is known that the frequency of electromagnetic radiation, moving toward or away from a stationary observer differs from that of the stationary source and is connected with it when $v_r \ll c$ by the following relationship:

$$f = f_0(1 \pm \frac{v_r}{c}) \qquad (1.7)$$

$f_0$is frequency of the signal emitted by a stationary source; f is frequency of the same source moving relative to the observer; v_r is the projection of the velocity of the source relative to the observer; c is the speed of light.

When the lens is moving relative to the stationary transceiver, the above formula becomes:

$$f = f_0(1 \pm 2\frac{v_r}{c}) \qquad (1.8)$$

and the Doppler frequency change due to the motion of a lens towards the measurement setup is respectively

$$\Delta f = f_0 \frac{2v_r}{c} = \frac{2v_r}{\lambda} \qquad (1.9)$$

One of the first installations for the RCS measurements of symmetric bodies is described in [4]. Diffuser on it was moving in a straight line and steadily.

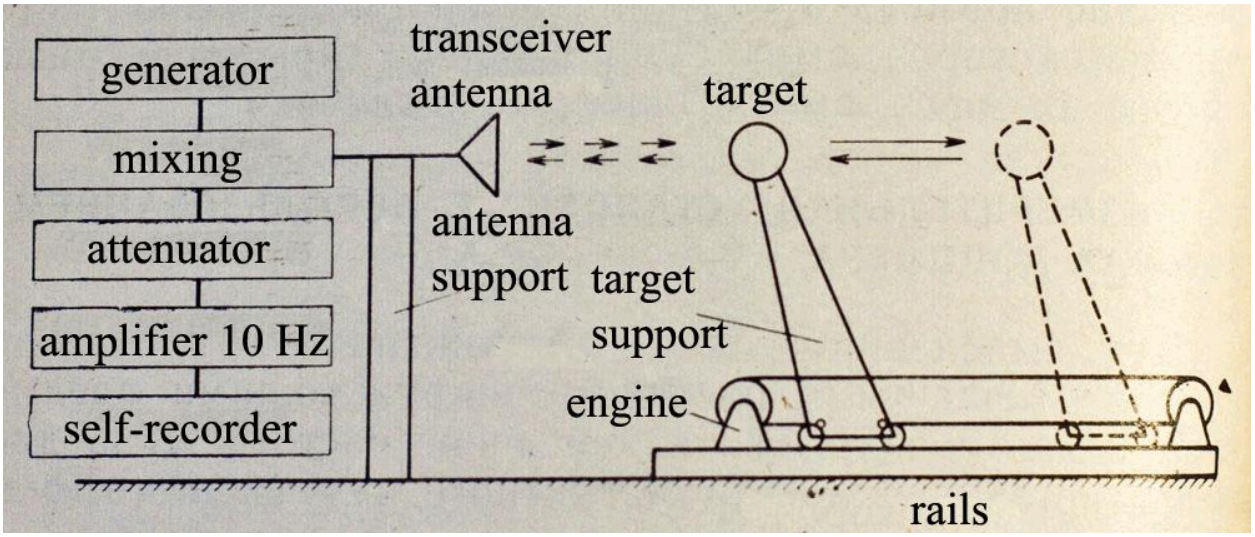

Figure 1.1 Block diagram of the measuring device using the Doppler effect.

The difference frequency signal that scattered by the target was selected. Amplitude is proportional to the field strength. Extra reflection was allocated by narrowband low-frequency amplifier. Low speed of the object led to a small value of the Doppler shift, which caused difficulties in the development of narrow band amplifier LF. It took a long time for the measurements.

To increase the speed of measurement, circular movement can be applied for the target. Such device is described in [5]. The magnitude of the radial velocity component varies as $v_r = vcos(\theta)$, where v_r is projection of the velocity vector on the line connecting the object and the transceiver, v is the circular velocity, θ is angle between v_r and v. On the opposite end of the test object supports the rotation mechanism fixed reference diffuser rotating together with the test object. To isolate the reflection from the target and reference scatterer, communicator is used, which ensures at every moment only one irradiation object.

These settings allow you to measure the RCS of only axisymmetric bodies. In RCS measurements for not axisymmetric bodies it is necessary to use a rotation

mechanism, which has been successfully used in the installation, which took place with the help of the measurements described in this paper.

RCS measurements on installations using the Doppler effect can significantly reduce reflections from stationary objects. Decreases the influence of the field inhomogeneity, illuminating an object on the error, since the movement of the object being studied averaged field, the effect of random variations of the field decreases. The method does not require complex electronic equipment other than the narrow-band low-frequency amplifiers.

1.5. Variations in measurements of the scattered waves

Measuring the RCS as biases errors and errors that have a random character are emerge.

The main source of systematic errors is that the incident wave on the lens is not perfectly flat, due to the finite distance between the measuring assembly and the object reflections between diffuser and support, and other reasons.

Often it is able to compensate systematic errors, or turning them into random using reducing by repeating RCS measurement chart and determine the average. Just depends on the systematic error standard of lenses, which conducted the calibration measurement setup.

Random error have the same significant role. The source of these errors are random noises of the receivers, ambient temperature changes, power supply instability, vibrations lenses when driving on the test plants and others.

2. DESCRIPTION OF LABORATORY EQUIPMENT

2.1. Laboratory-scale plant

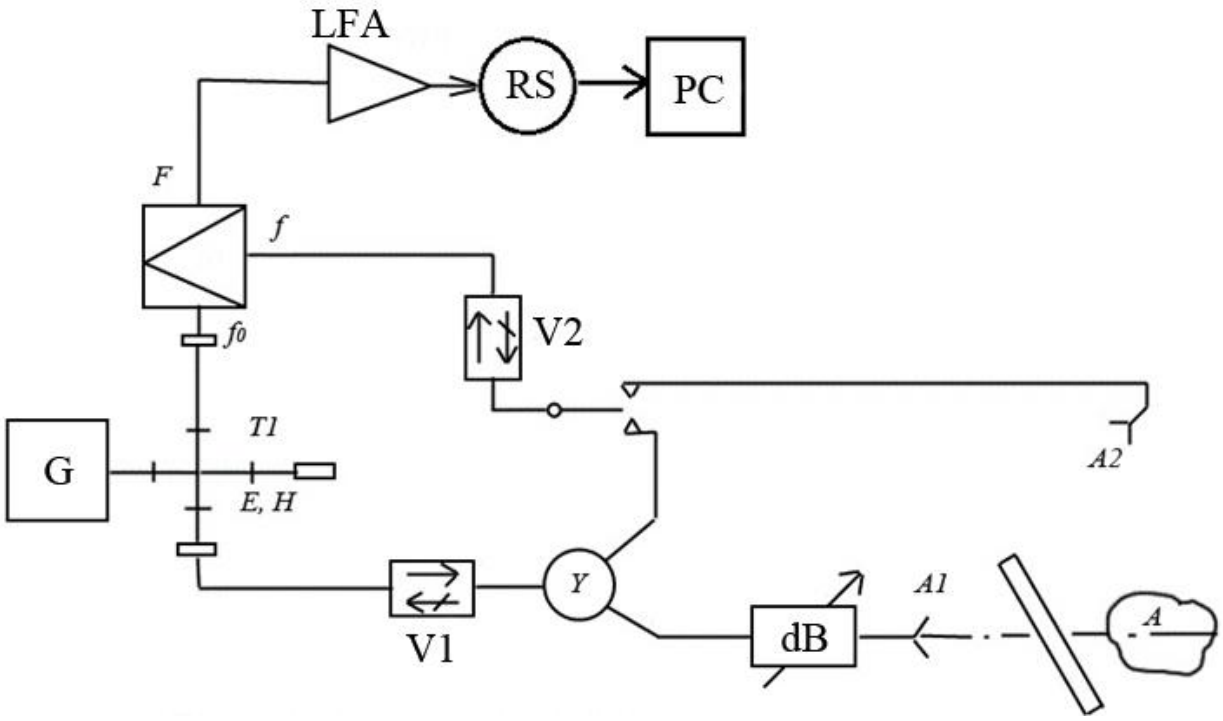

Figure 2.1. The scheme of the laboratory setup

The signal reflected from the object A is received by antenna A1. Mixing reference signal with reflected is made by the balanced mixer BS to the output of which is placed a narrowband bass amplifier tuned to the frequency of the Doppler shift. Gates B1, B2 and Y circulator are included for unleashing receiving and transmitting channels. Crank mechanism allows to fix on it the object studied

reciprocating motion. The waveguide has an internal section 16 x 8 mm that corresponds decimeter wavelength range.

Calibration is executed using a layout attenuator Y, which is included immediately before the transmitting antenna.

The block B1 is composed by the 90-degree bridge and the two detectors for which the sum comes to the reference and the reflected signal. Further data enter the connected card NI-6008, and the digitized signal is processed on a PC program LabView.

The engine driving the crank mechanism is closed in rectangular sinks, so they arranged for the purpose to reduce the reflection from the object.

Exterior installation is shown in Fig. 2.2. Input board NI-6008 is not connected.

Figure 2.2. Exterior view the installation without board input.

Crank mechanism with a view is shown in Figure 2.3.

Fig. 2.3 The target, mounted on the mechanism of movement.

2.2. Devices geometry and specifications

Microwave generator

To generate a microwave signal generator G4-108 is used and tuned to 14.85GHz.

The main technical characteristics of the device G4-108:

Frequency range: 12.16 - 16.61 GHz
Limits of basic frequency setting error: ± 0.1%.
Frequency instability for 15 min $\pm 1 * 10^{-4}$.
Spurious frequency deviation of not more than $2 * 10^{-5}$.
Output Level: ($1 * 10^{-3}$ - $1 * 10^{-14}$Vt) 0 ... -110 dB.
The instability of the reference output level for 15 min: ± 0.1 dB.
Output accuracy set the reference power level ($1 * 10^{-3}$ W) ± 0.5 dB.

Settings for the internal modulation "meander":
repetition rate of 1 kHz ± 0.1;
unevenness of peaks: 10%.

Parameters of the external IM:
repetition rate: 0.25-10 kHz;
amplitude of 5-10 V;
duration: 0.2-10 ms;
rising and falling less than 0.1 ms and 0.2 ms respectively;
unevenness of peaks: 10%.

Parameters of the output signals of MI:
the rise time is less than 0.1 ms;
length of cut no more than 0.2 ms;

temporal instability of the pulse duration is not more than 0.1 ms;
uneven peaks of the envelope is more than 20% (for pulses of duration 0.5 ms).

Parasitic AM no more than 1% (in CW mode);
Output VSWR less than 1.3.
Mounting dimensions RF output - waveguide section 16x8 mm.
Power supply: 220 ± 22, 50 ± 0.5 Hz.
Power consumption: 150 A.
Replaces: G4-11A, G4-32A
Recommended replacement: G4-198A, G4-198
Analogue: HP 83711B
Weight 31 kg.
Dimensions: 530 x 330 x 318 mm.

Attenuator

D5-4 attenuator absorbs.
Operating frequency range 12-16.6 GHz
Available attenuation 0 ... 50 dB + 2%

Signal acquisition channel:

Before the input card NI-6008 amplifier bandpass filter of the first order is placed with a restriction on the lower frequency 10Hz to 200Hz at the top.

To enter data into the computer and post-processing in LabView, it is used capture card NI USB-6008/6009 (Figure 2.4). It is connected to PC via full-speed USB interface and contains eight channels of analog input (AI), two channels generate analog signals (AO), 12 channels of digital I / O (DIO) and the 32-bit counter[6].

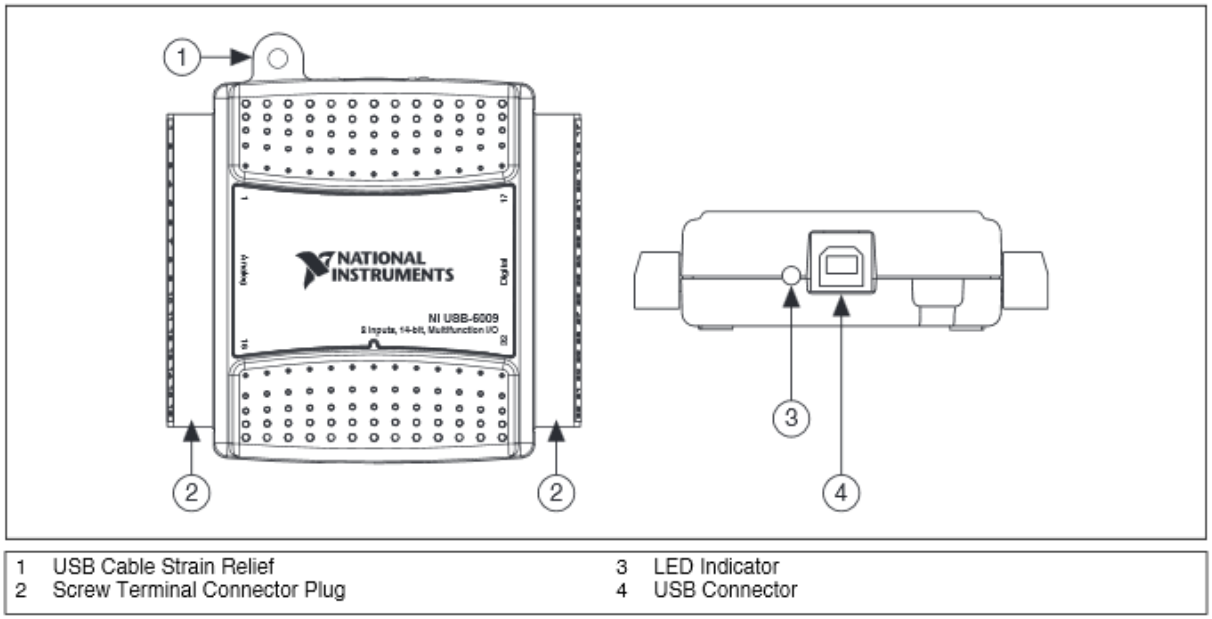

1	USB Cable Strain Relief	3	LED Indicator
2	Screw Terminal Connector Plug	4	USB Connector

Fig 2.4. NI USB-6008/6009 Top and Back Views

External Voltage

+5 V output (200 mA maximum)

Minimum .....+4.85 V

Typical.....+5 V

+2.5 V output (1 mA maximum) .....+2.5 V

+2.5 V accuracy .....0.25% maximum

Reference temperature drift .....50 ppm/°C maximum

Event Counter

Number of counters 1

Resolution .....32 bits

Counter measurements.....Edge counting (falling-edge)

Counter direction .....Count up

Pull-up resistor .....4.7 kΩ to 5 V

Maximum input frequency.....5 MHz

Minimum high pulse width.....100 ns

Minimum low pulse width .....100 ns

Input high voltage .....2.0 V

Input low voltage .....0.8 V

Bus Interface

USB specification .....USB 2.0 full-speed

USB bus speed .....12 Mb/s

Power Requirements

USB

4.10 to 5.25 VDC

Typical.....80 mA

Maximum.....500 mA

USB suspend

Typical.....300µA

Maximum.....500µA

Physical Characteristics

Without connectors .....63.5 mm × 85.1 mm × 23.2 mm (2.50 in. × 3.35 in. × 0.91 in.)

With connectors .....81.8 mm × 85.1 mm × 23.2 mm (3.22 in. × 3.35 in. × 0.91 in.)

Figure 2.5 shows key functional components of the NI USB-6008/6009.

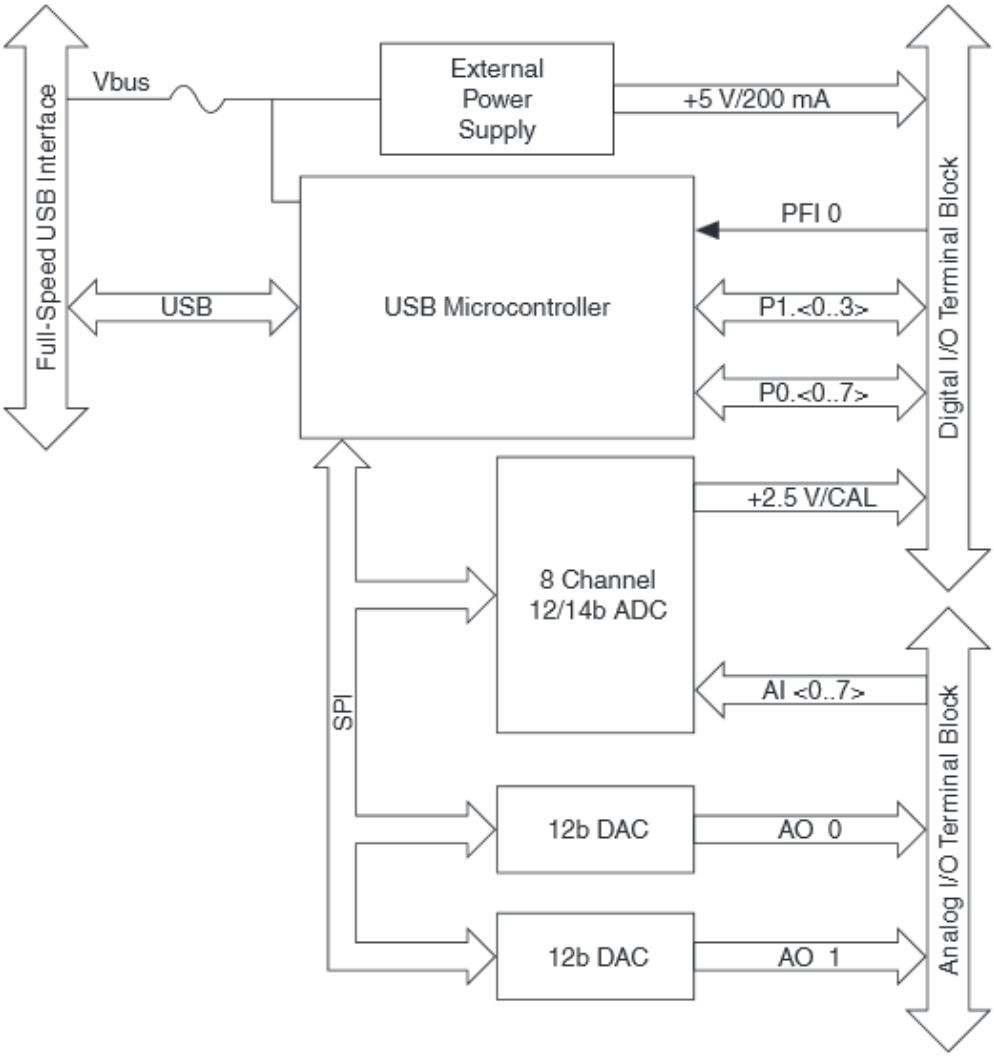

Fig.2.5 Functional components of the NI USB-6008/6009.

For visualization and data-processing LabView package is used. The main advantage of this package is that you can write in LabView rather complex program and implement various algorithms measurement, control and data processing, using a graphical interface and without having professional knowledge of programming languages.

2.3 Horn antenna transceivers

We studied two pyramidal horn antennas, operating in two-centimetric wavelengths. For them we got radiated pattern in E and H - planes in order to evaluate the distribution of the field in the measurement objects. From these radiation patterns we found that the field distribution in the measured objects is evenly.

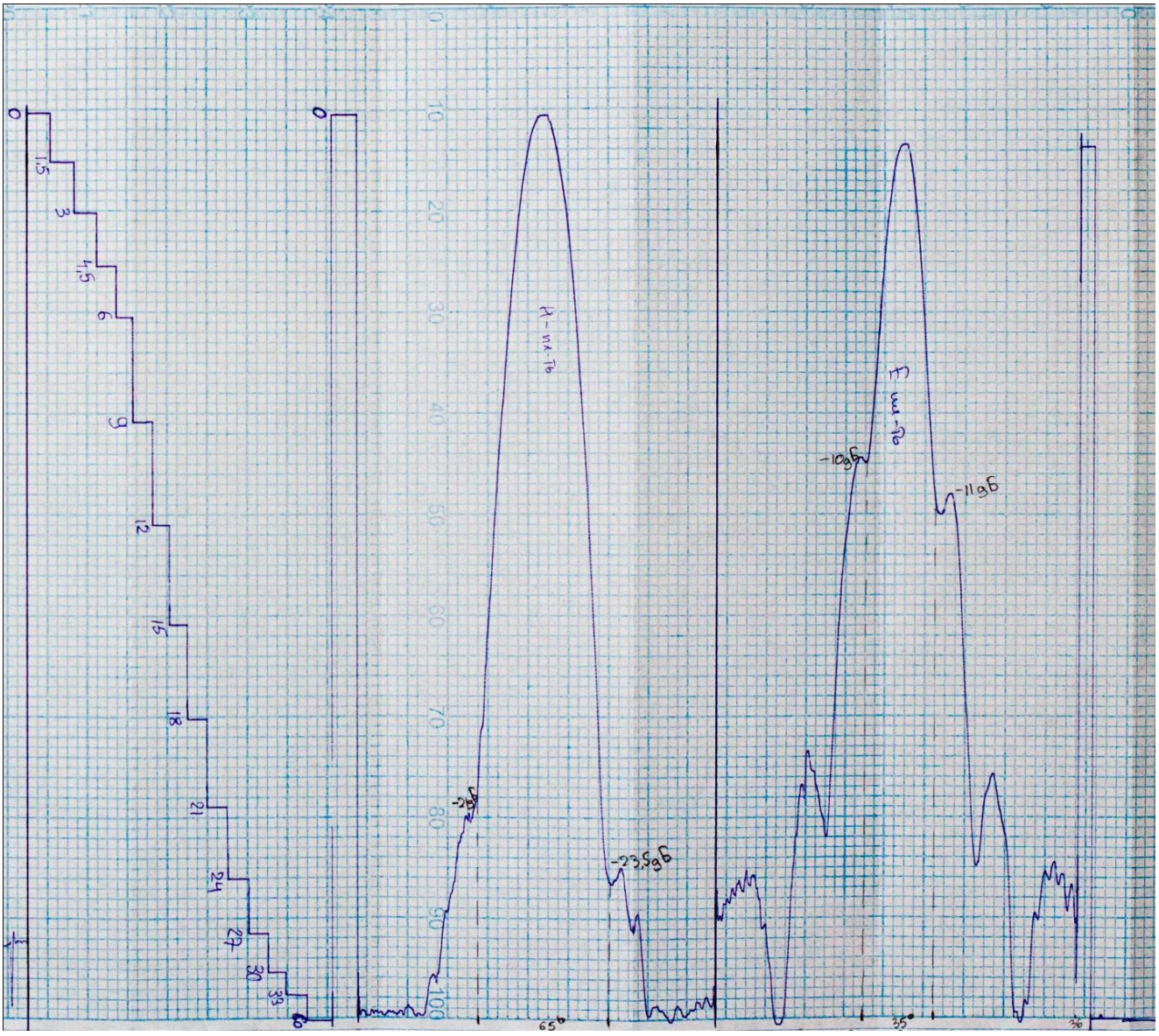

Figure 2.6 The radiation patterns in the H and E-planes for the pyramidal horn a = 50 mm, b = 60 mm.

Table 2.1.

Polarisation	width -3dB	sidelobes
H	65^0	-21dB, -23.5dB
E	35^0	-10dB, -11dB

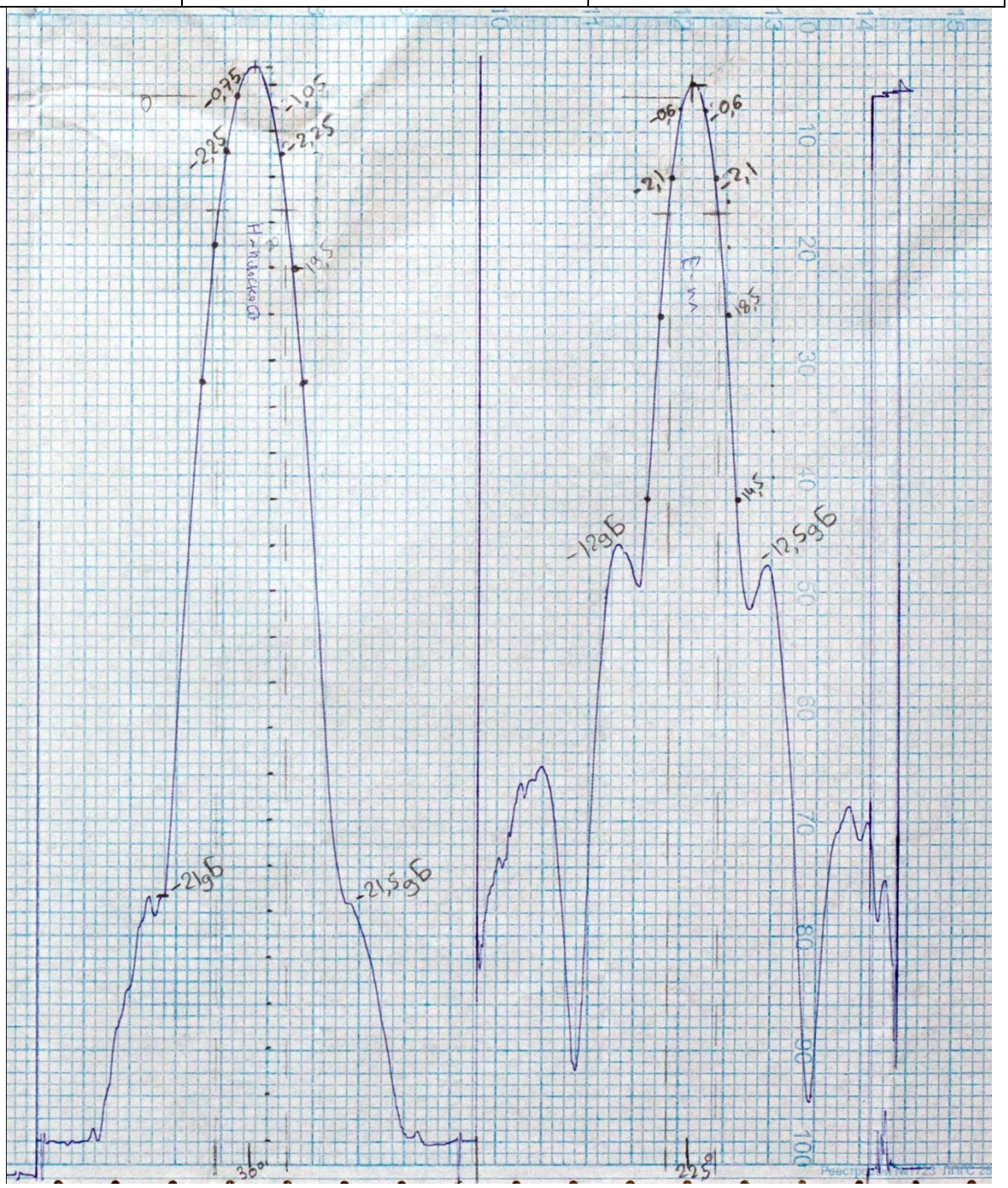

Figure 2.7 The radiation patterns in the H and E-planes for the pyramidal horn a = 50 mm, b = 60 mm.

Table 2.2.

Polarisation	width -3dB	sidelobes
E	30^0	-21dB, -21.5dB
H	22.5^0	-12dB, -12.5dB

3. SIGNAL MODELING OF RF DETECTOR

3.1. Calculation of the phase change signal

For the motion of the object the crank mechanism is used. Making the equation of motion for the target and knowing the size of the mechanism, we can calculate the phase shift vector intensity reflected from the target.

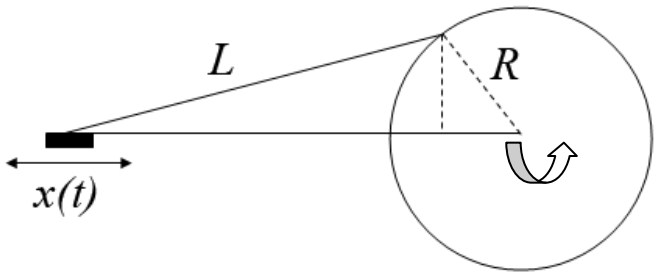

Figure 3.1 The geometry of the mechanism of movement.

$$x(t) = \sqrt{L^2 - R^2 + R * (\cos^2 \varphi(t))} - R * \cos(\varphi(t)), \quad (3.1)$$

Where φ = w * t is the angle, x (t) is the distance from the rotational axis to the slide. Calculation of parameters is performed in one period.

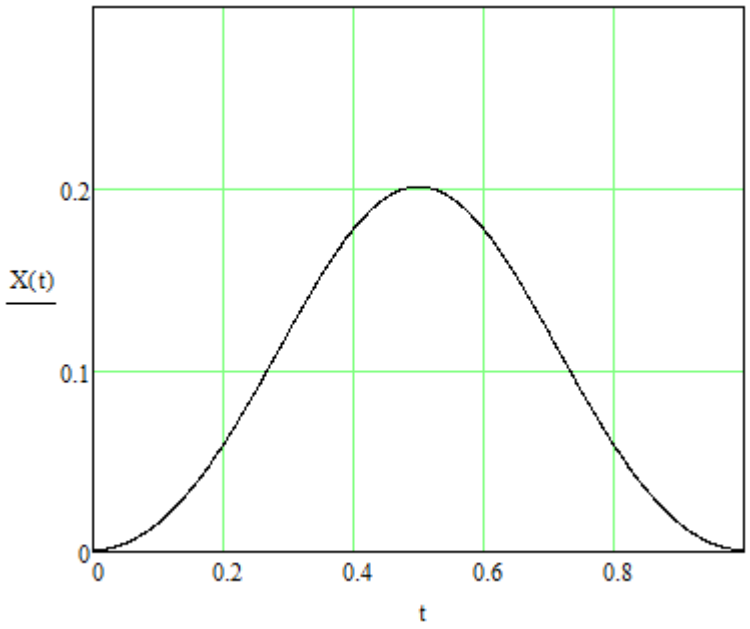

Figure 3.2 Changing of the distance from the axis of rotation to the slider.

Phase of the reflected signal varies in accordance with:

$$\Psi(t) = 2 * \frac{x(t)}{\lambda} * 2\pi \qquad (3.2)$$

Taking the derivative of phase with respect to time we obtain a frequency shift of the phase change:

$$W(t) = 2 * \frac{w}{\lambda} * R * \sin(w * t) * (1 - \frac{R*\cos(w*t)}{\sqrt{R^2*\cos^2(w*t)+L^2-R^2}}) \qquad (3.3)$$

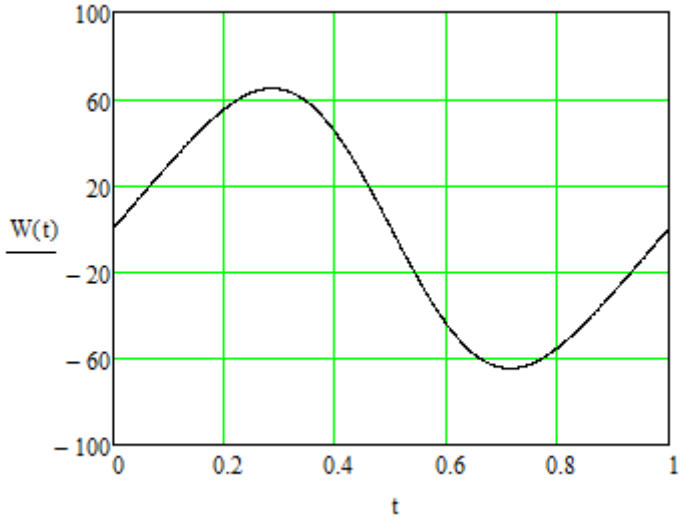

Figure 3.3 The frequency shift of the phase change for one period.

3.2. The detector signal with the phase of the reference and reflected signals

At the output of the 90-degree bridge the reference ($\overrightarrow{E0}$) and the reflected ($\overrightarrow{E1}$) signals are added in each channel waveguide based on phase. Consider a single channel. The amplitude of the vector sum of the intensity $\overrightarrow{E01} = \overrightarrow{E0} + \overrightarrow{E1}$ can be seen in Fig. 3.4. The blue curve shows the vector sum of the module when at the initial time they have the same direction. The red curve corresponds to the vector sum when the initial time they are perpendicular to each other. Graphs are separated in amplitude for readability. All other relations are possible (their initial phasing). Ratio of the amplitudes of the reference and the reflected waves 1: 5.

The detector output signal (on bass) can be calculated by considering a quadratic or linear transfer characteristic.

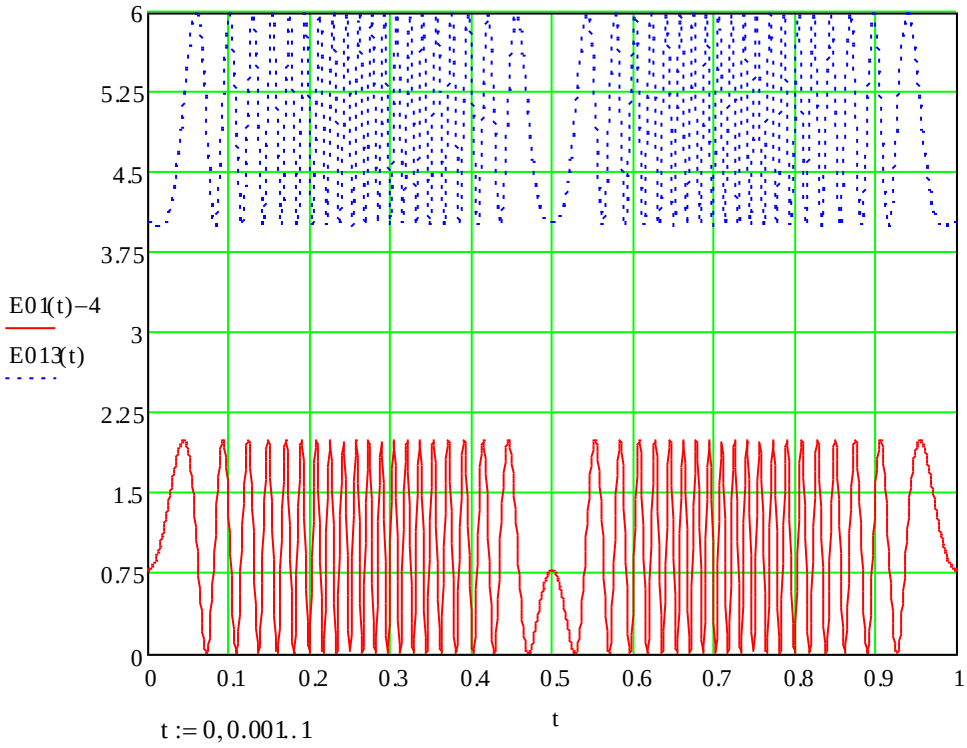

Fig. 3.4 The simulated signal.

3.3 Simulation of bandpass filtering of the signal from a detector

The signal received from the detector of the experimental setup passes through a bandpass filter to select only the useful signal component, eliminating unnecessary components and increasing the signal / noise ratio.

A simple band pass filter can be regarded as a resonance amplifier based on the LC-circuit. The transfer coefficient is represented as *K (jw) = K0 / [1 + jQ (w / w0 - w0 / w)]*. At a frequency equal to the resonant w = w0 the maximum transmission rate is equal to *K0*. The value of *Q* – *Q* is factor of the resonance curve (the value of *Q* is chosen 10..20, depending on the required bandwidth). Calculations using a fast Fourier transform (FFT) of the transition from *w*(frequency) to *n*(number), *w0 = n0* (near 250).

The spectrum S (n) of the signal s (t) with zero mean value (4096 samples in the signal are used) is multiplied by K (jn), inverse FFT is then performed. We obtain a filtered signal $s_f(t)$ (4096 samples) and build graphs $s_f(t)$ for all values of the initial phase. It is important to pay attention to the amplitude of the filtered signal $s_f(t)$. It will depend on the initial phase. The transition process in this case is not modeled, it will be taken into account when creating a virtual device environment LabView.

The chart shows the module gain K (jn) = K0 / [1 + jQ (n / n0-n0 / n)] with n0 = 250 and n = 1..4096 for different quality factor Q = 10,15 and 20. The higher the quality factor, the narrower the bandwidth. Bandwidth is equal to 25.25 for Q = 10 and 17.39 for Q = 15.

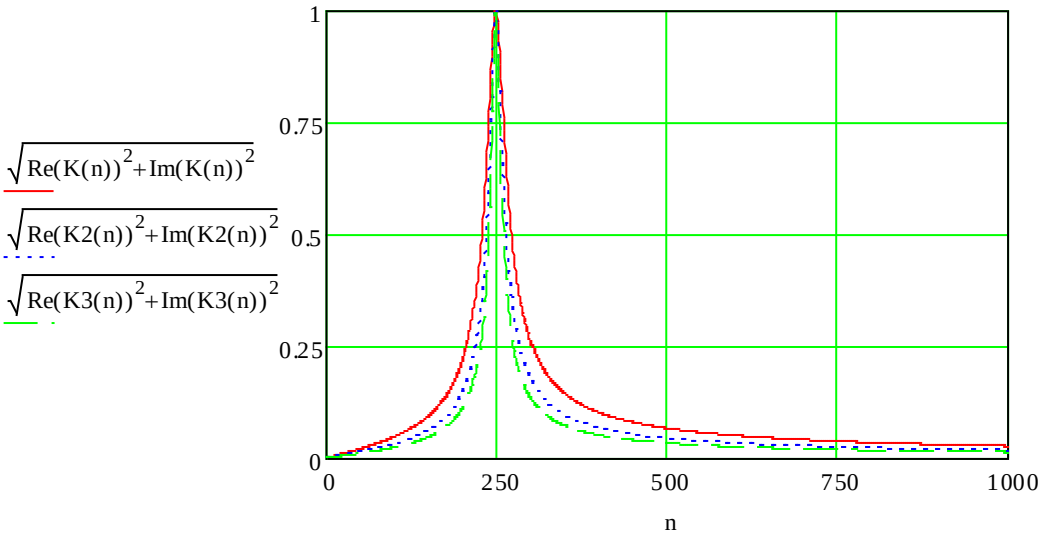

Figure 3.5 Frequency response of the filter for different Q.

Spectra of simulated signals with different initial phasing of the reference and the reflected signal, the frequency response in the above form (n0 = 250, Q = 15):

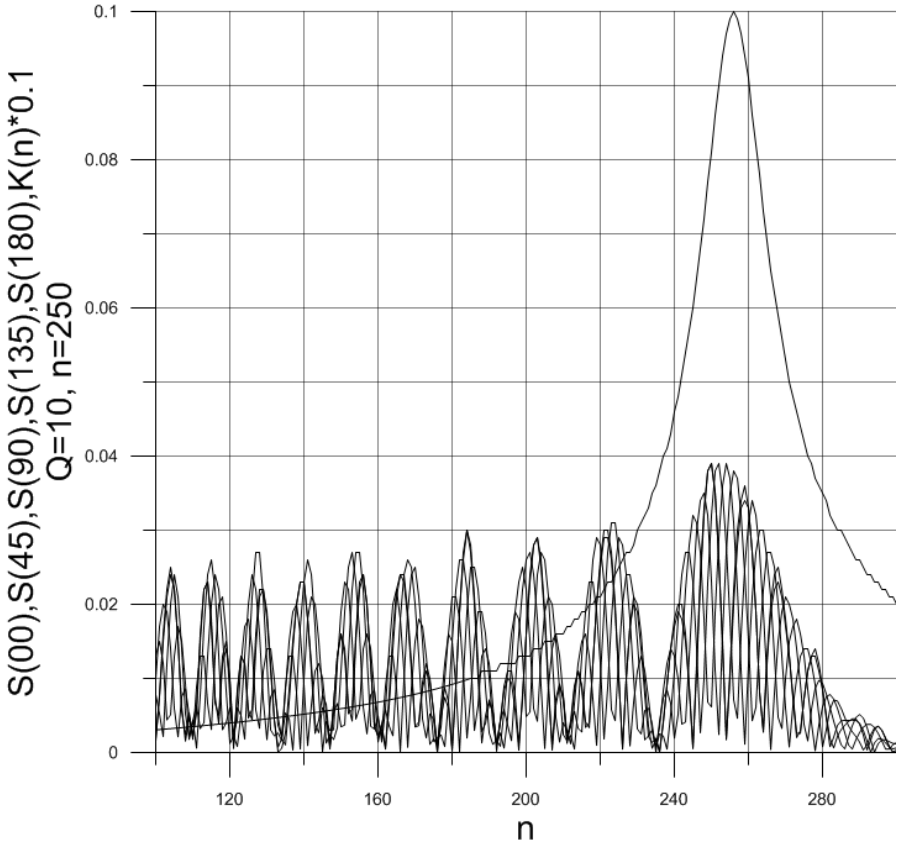

Figure 3.6 Spectra of the simulated signal and the frequency response of the filter.

Next in the signal exist a 50Hz interference caused by surrounding electrical appliances and wiring. Simulated signal takes the form:

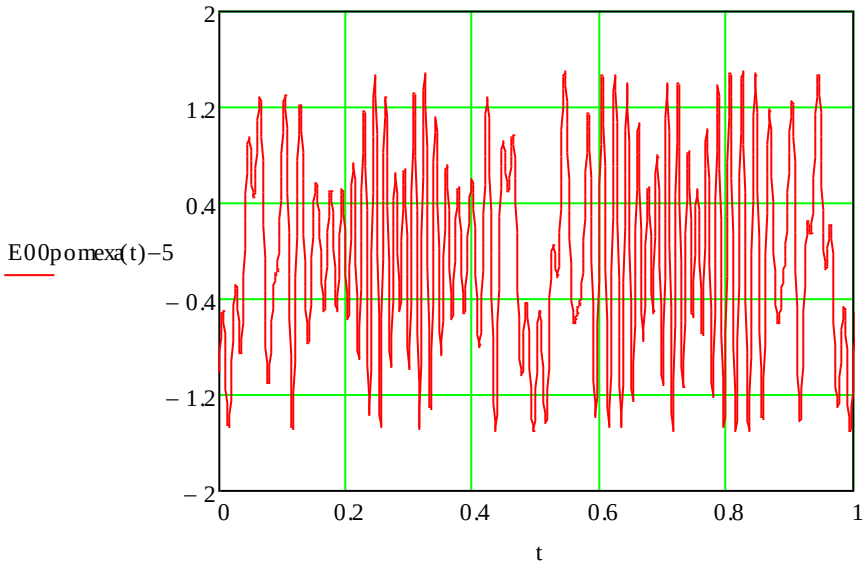

Fig. 3.7 Graph of the simulated signal with interference, minus the constant component.

The spectrum of this signal has the form:

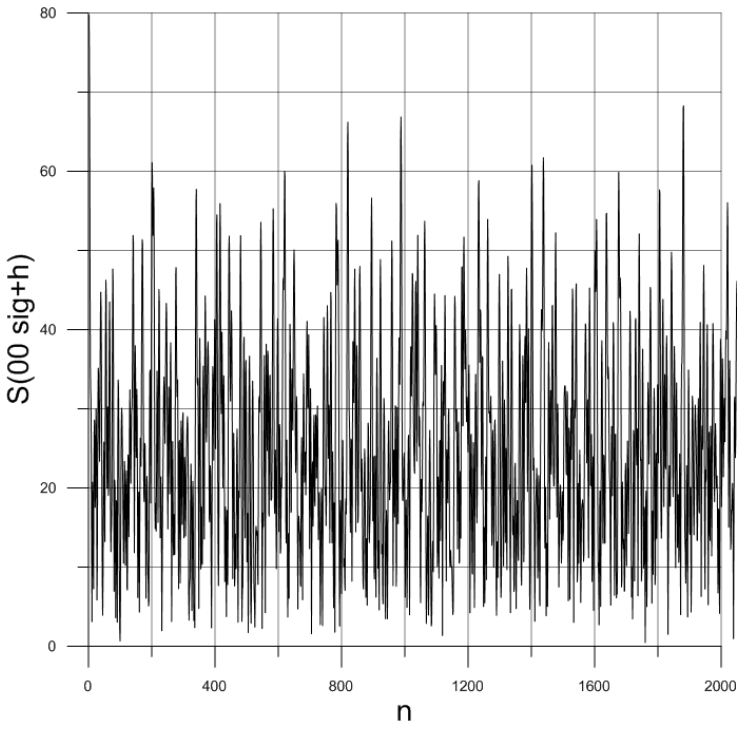

Fig. 3.8 The spectrum of the simulated signal with noise.

Restored using inverse Fourier transform signal after filtering with n0 = 255 and Q = 10, inverted relative counts:

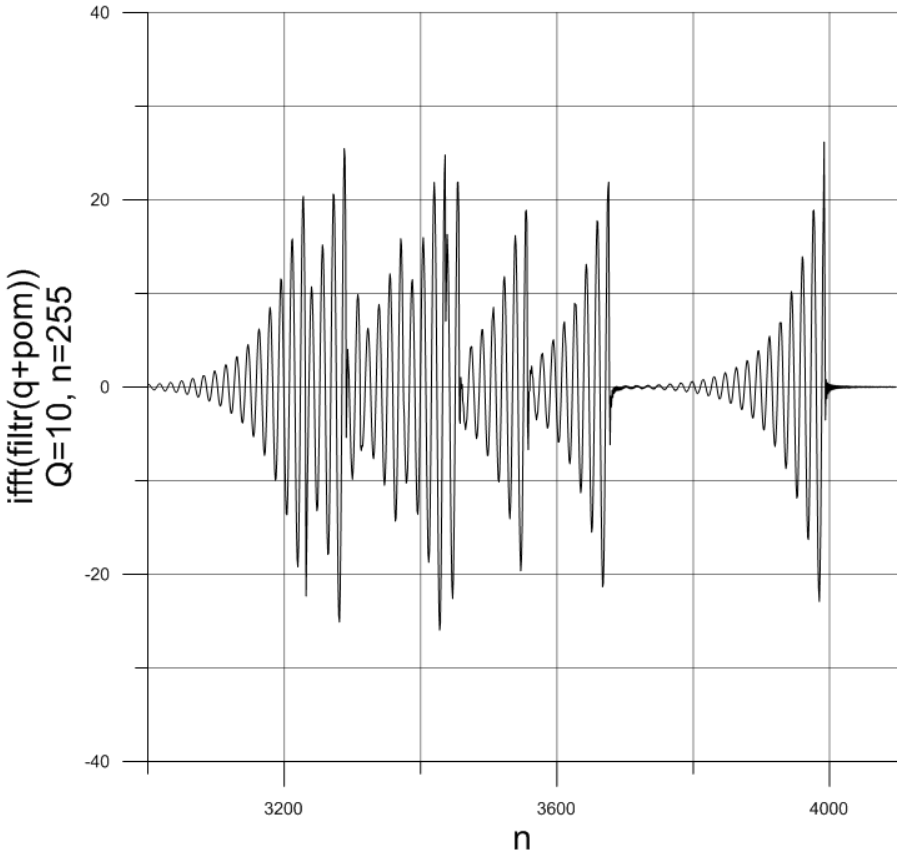

Fig. 3.9 Recycled inverted signal.

The presence of transients in the detected signal does not allow to distinguish the desired signal after using VLF filter. Therefore a new method of data processing, described below, was developed. It was named synchronous detection.

4. MEASUREMENTS

4.1. Registration of signals

As a result of measurement using virtual instrument software LabView, the detector signals were observed visually on a virtual oscilloscope and were written to a file.

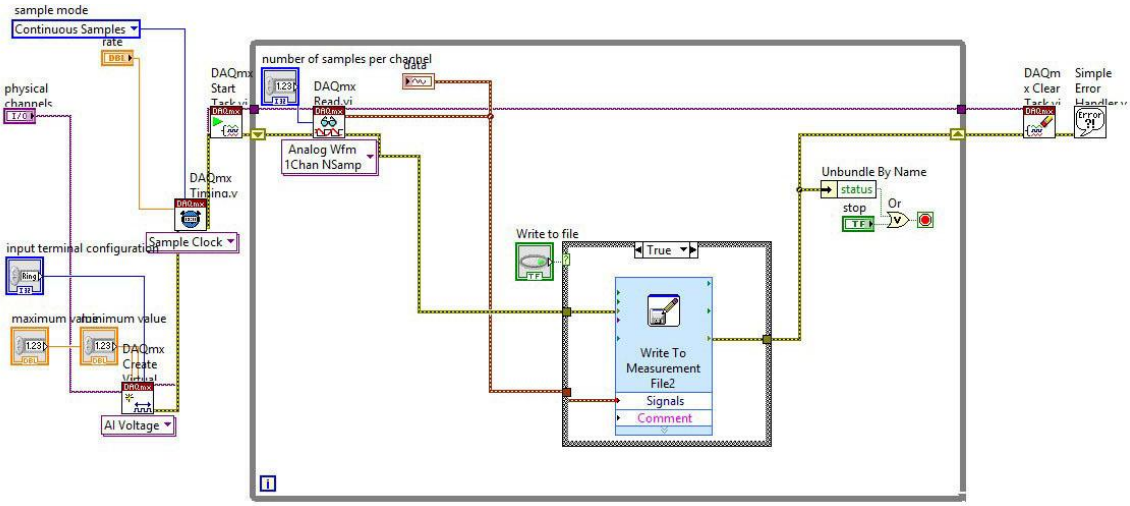

Fig. 4.1 Scheme of VIs in LabView.

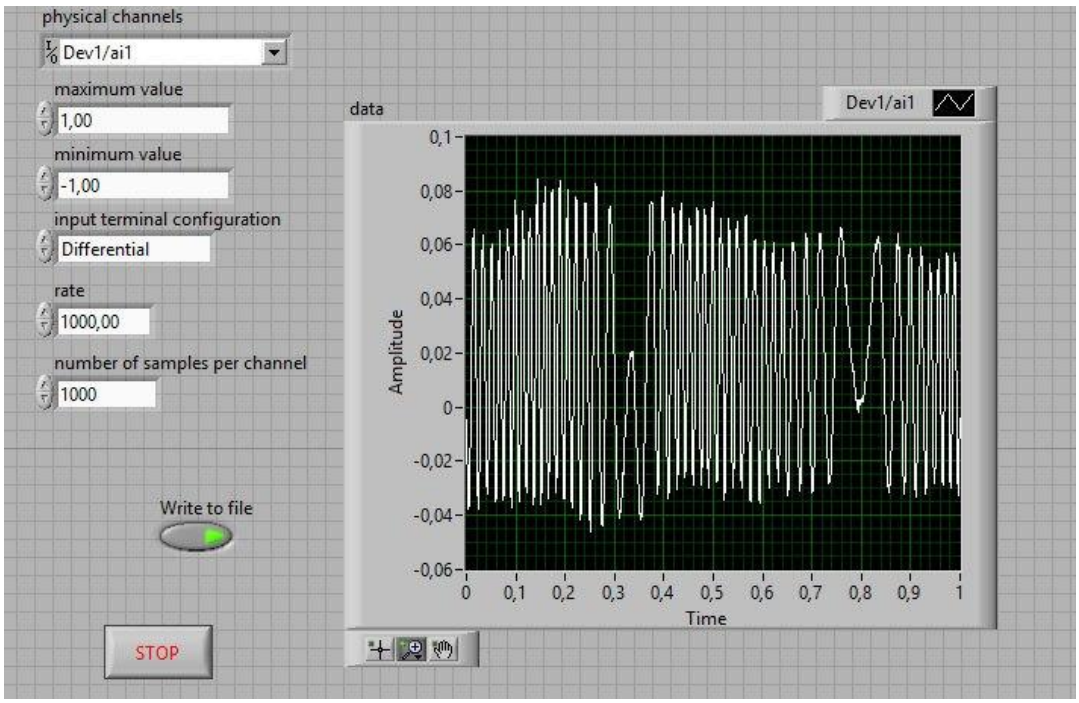

Figure 4.2 The program interface registration signal in LabView environment.

When measuring the RCS of the corner reflector and a spherical segment, the data is recorded by two detectors at the same time.

When measuring the RCS of the cylinder, due to peculiarities of the board NI-6008, it was necessary to go to the differential channels connection, thus reducing the input voltage range from ± 10V to ± 1V, allowing to record accurately a weak signal.

The figures 4.3. and 4.4. below show the difference between the signal from two detectors, as well as the signal at the maximum, average and noise.

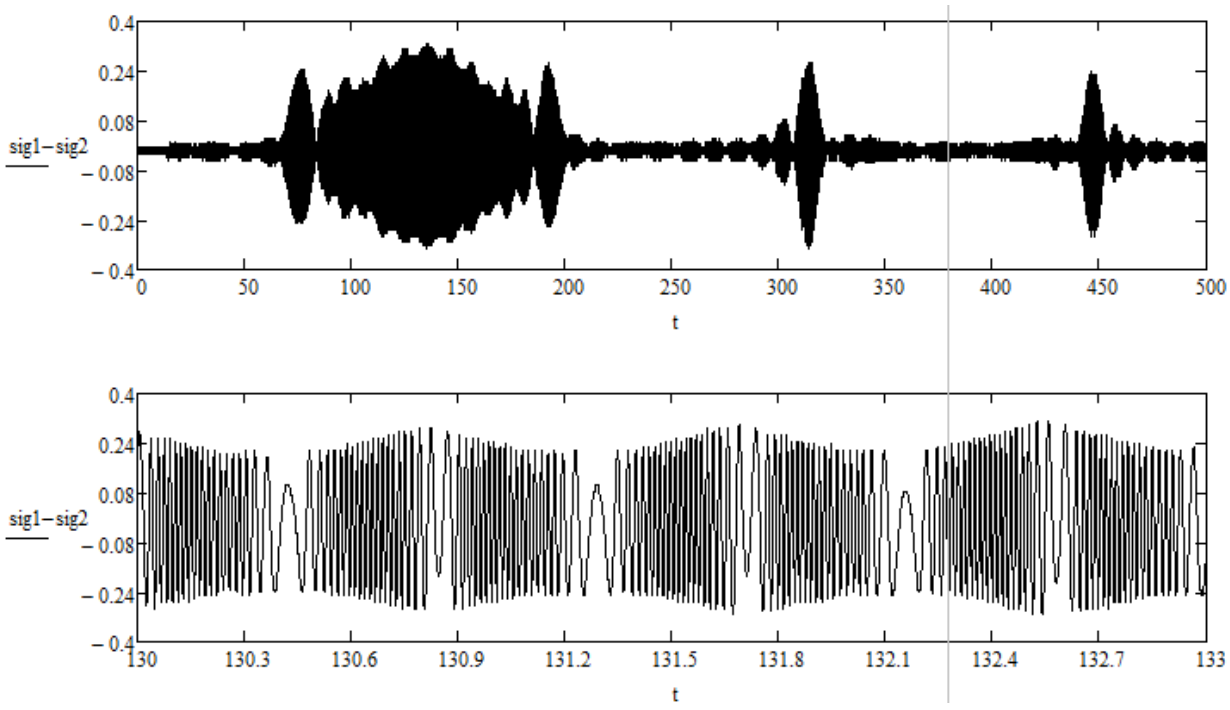

Figure 4.3 The detected signal, the signal is at its maximum.

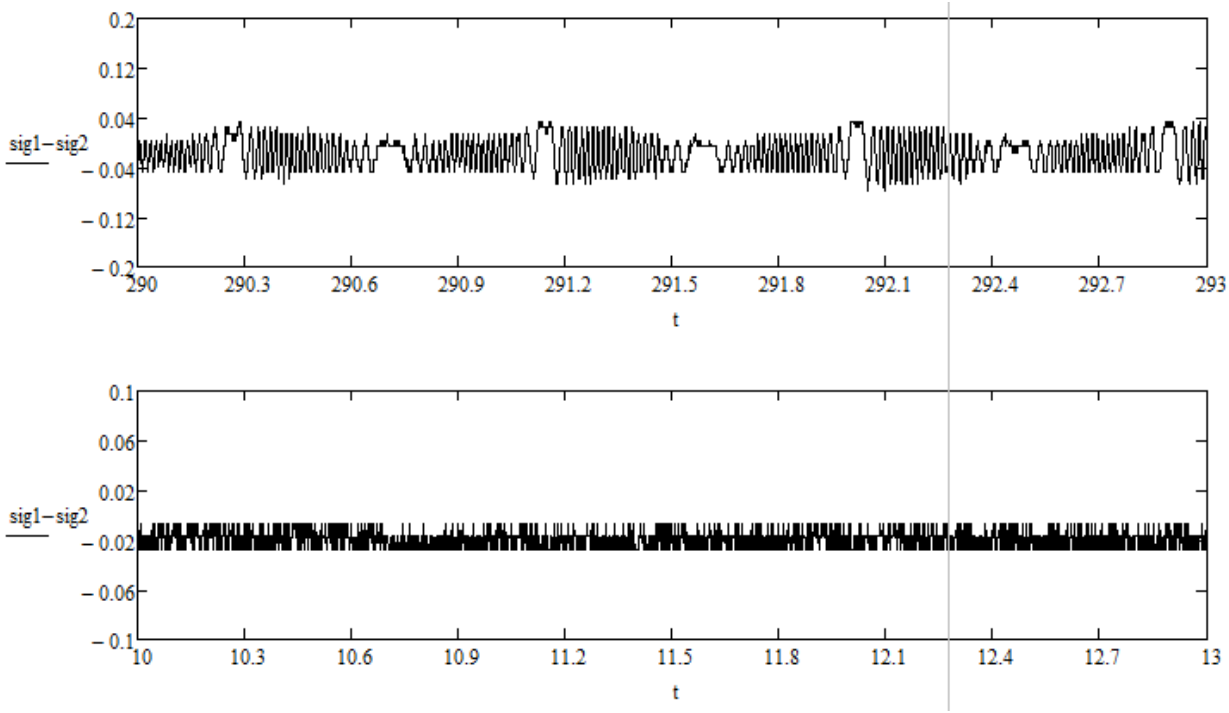

Figure 4.4 Weak signal, noise signal

4.2 Calibration of the system

Before the measurement was carried out calibration of the system with an attenuator using a meander signal. In place of a transceiver a pyramidal horn was placed a cap. The reference signal goes to detectors with the amount of the signal reflected from the stub.

The same calibration was performed with corner reflector. The generator was switched to continuous generation (CG), the rotation of the object was disconnected and the weakening was regulated by an attenuator. Calibration was performed for a signal having a gain of 0 dB and 7dB.

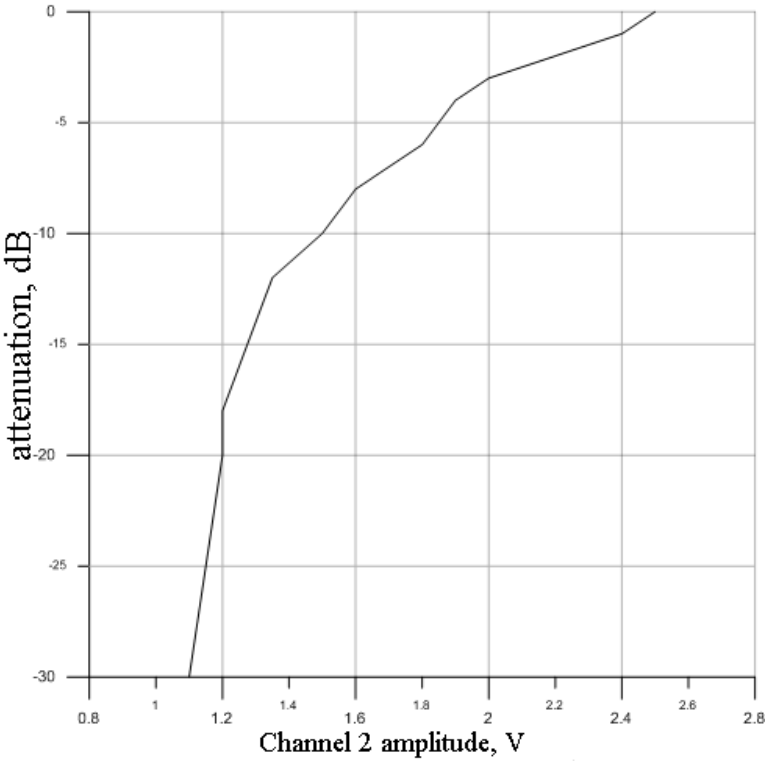

Fig. 4.5 Calibration using meander.

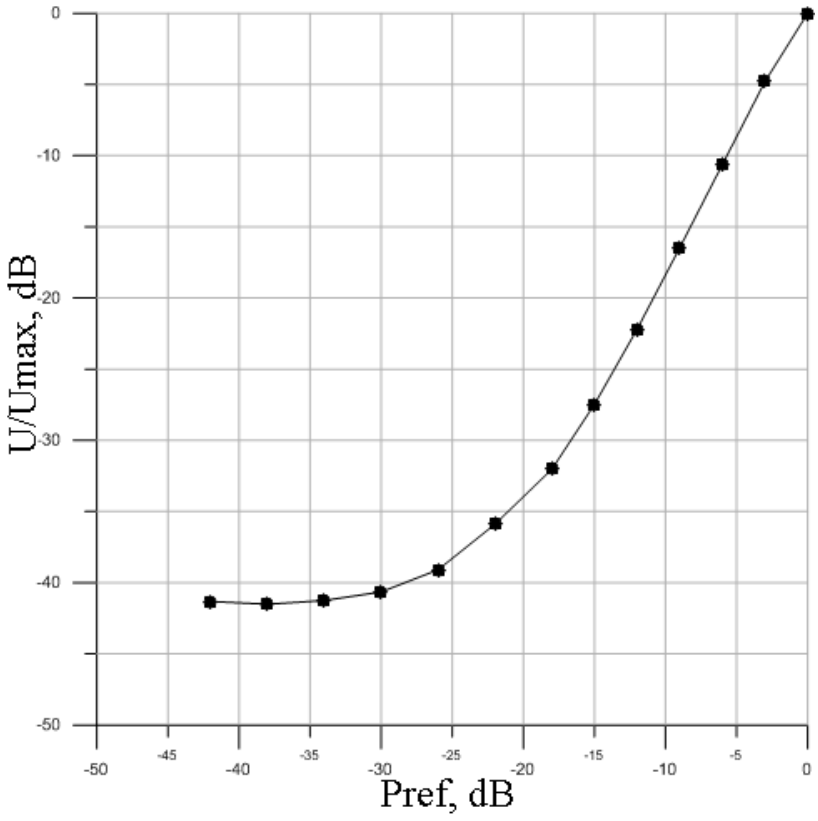

Figure 4.6 Calibration to 0 dB.

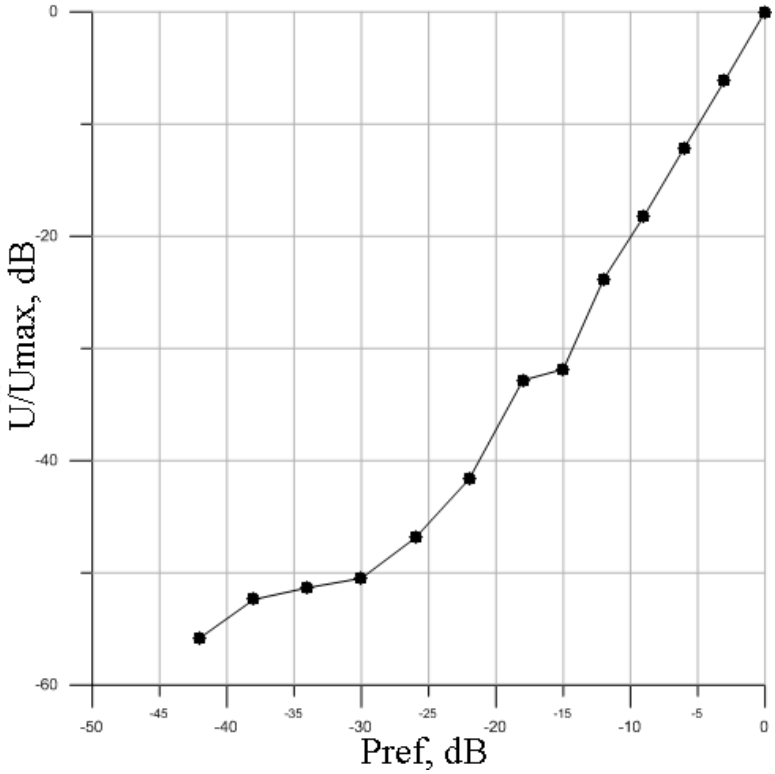

Fig. 4.7 Calibration for 7dB.

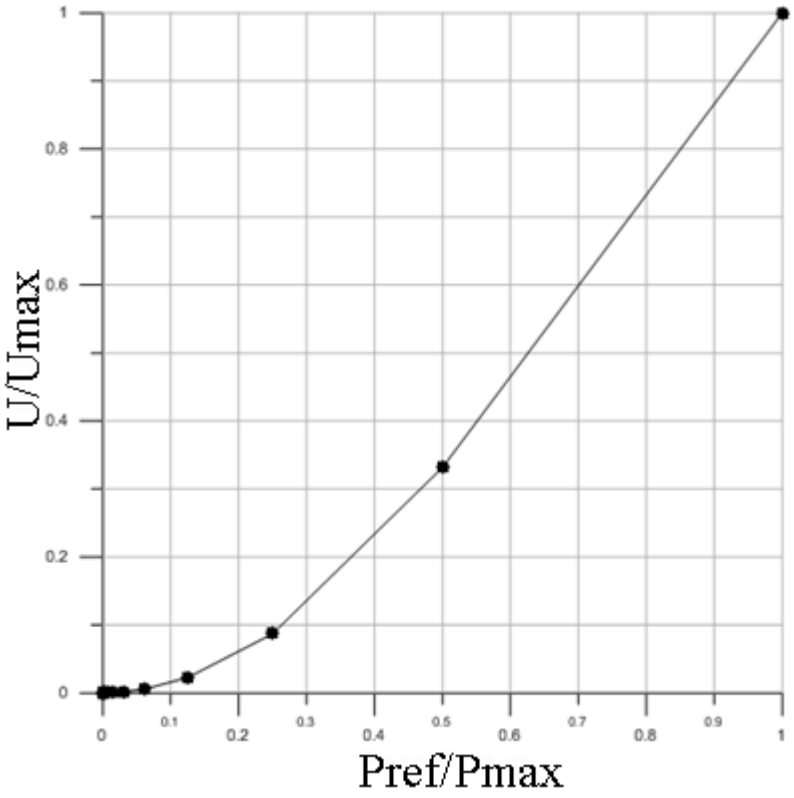

Fig. 4.8 Calibration to 0 dB.

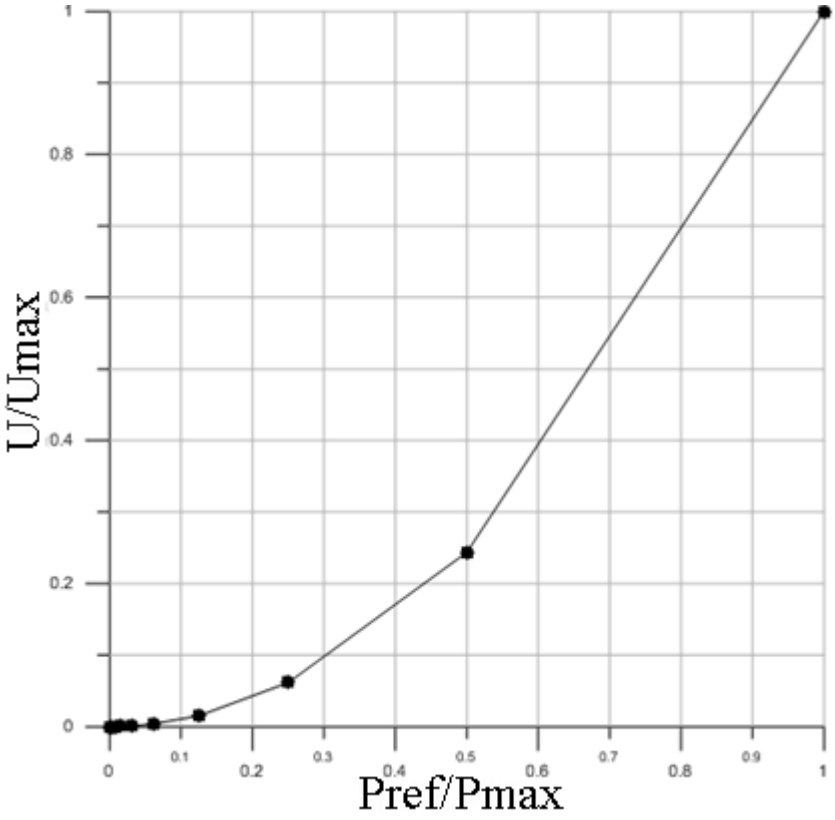

Fig. 4.9 Calibration for 7dB.

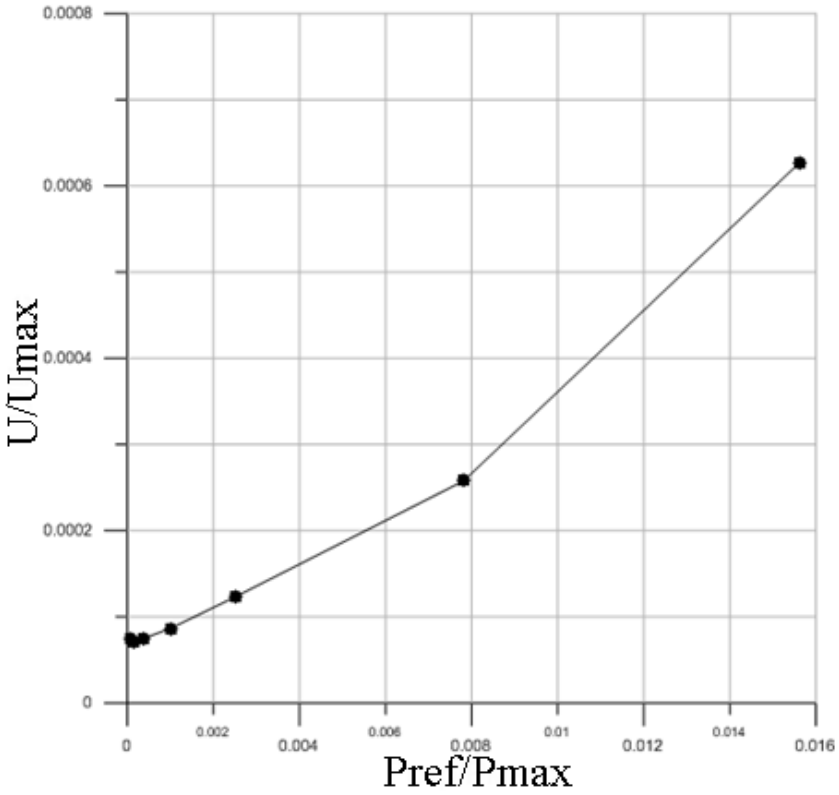

Fig. 4.10 Calibration to 0 dB for small signal.

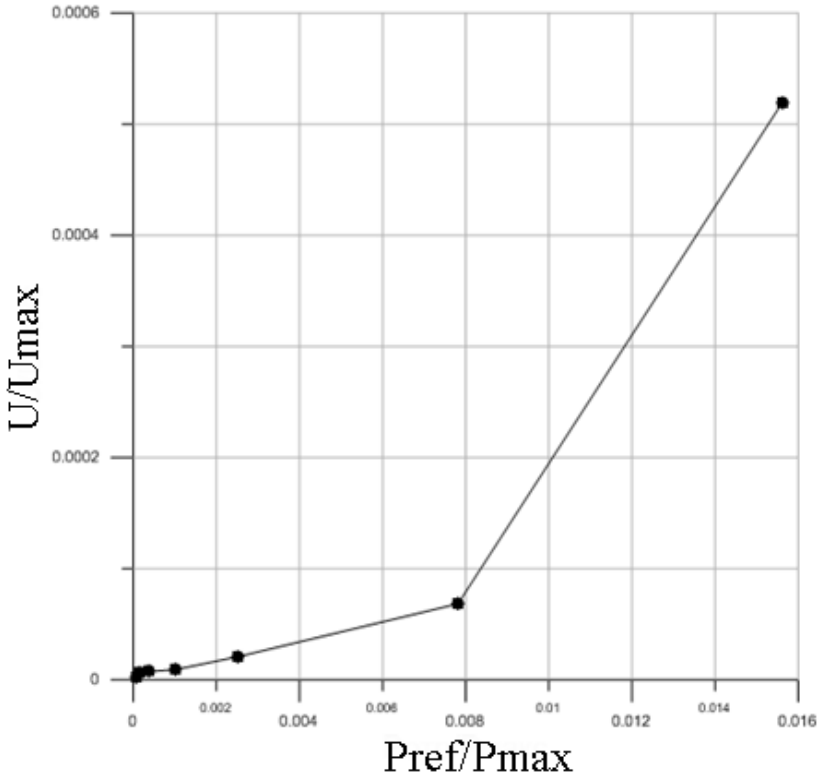

Fig. 4.11 Calibration 7dB for small signal.

4.3 Methods of Signal Processing

Since the use of ULF filter for processing the recorded signal in the simulation has not given the expected results, it was necessary to introduce new methods of data processing. The recorded signal consists of the desired signal and transients due to the fact that the purpose of moving on the mechanism falls into extreme positions, where slows and reverses direction. These transients can be seen on the chart below.

The body has a periodic motion, so one can calculate how many samples goes to a transition process and the desired signal. Transients can be blanked using a mask.

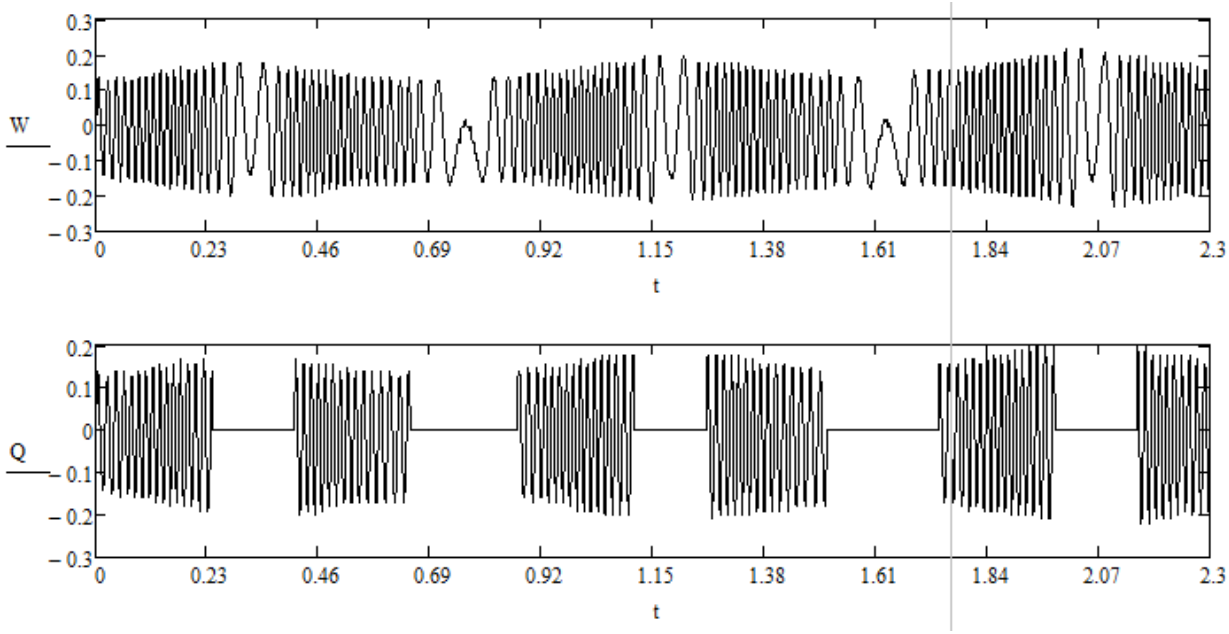

Fig. 4.10 Transients blanking

Further, a technique for synchronous detection with quadrature channels was developed. For this purpose, analyzing the spectrum portion of the desired signal, was found the maximum signal with frequency f = 68 Hz. Further, the value of the signal s (x) are multiplied by sin and cos of this frequency, and the components I_{cos} and I_{sin} calculated by the formulas:

$$I_{cos} = \int_T^0 s(x) * \cos(2\pi f t) dt \qquad (4.1)$$

$$I_{sin} = \int_T^0 s(x) * \sin(2\pi f t) dt \qquad (4.2)$$

The average amplitude of one portion of the desired signal is equal to:

$$A = \sqrt{I_{cos}^2 + I_{sin}^2} \qquad (4.3)$$

The obtained value is the amplitude, averaged over the time of object movement between the extreme positions. From time one can go to the angle of rotation as well as for the entire measurement the body turned a known number of degrees.

The maximum frequency of the useful signal changes with the speed of movement of the slider in the unit. However, all measurements were selected at optimum speed, so for all measurements the frequency was f = 68 Hz.

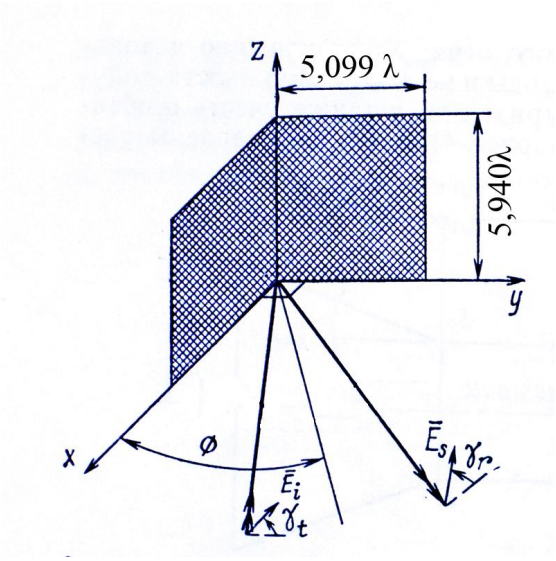

Fig. 4.11 Geometry of the test corner reflector

Starting readings on the graph corresponds to the position angle reflector, when the angle is $\phi = 0$ and $\gamma_t = \gamma_r = 0$ is horizontal polarization. Dimensions of the corner reflector are shown in Fig. 4.11.

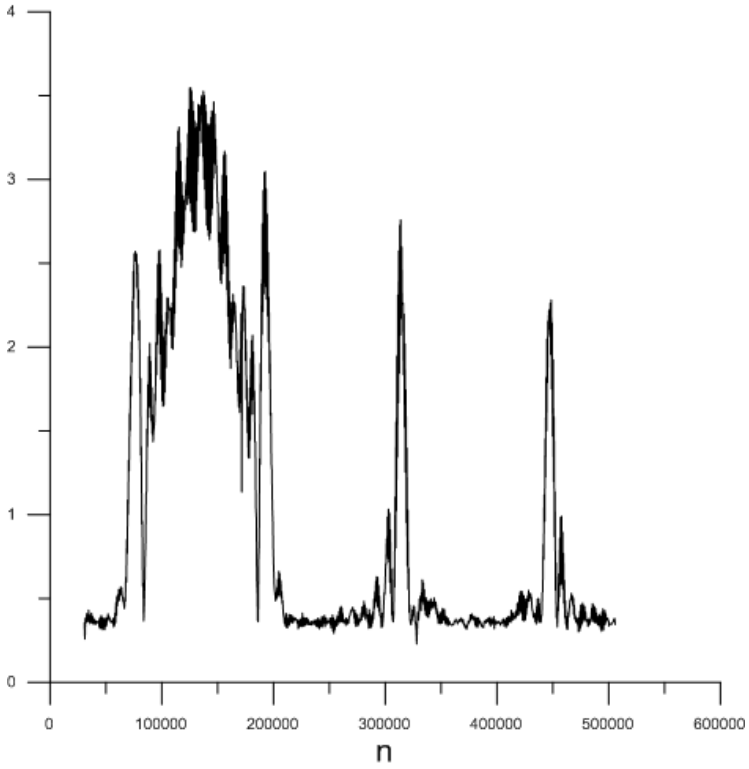

Fig. 4.12 The dependence of the signal amplitude on the rotation angle (by number of reference) for a corner reflector.

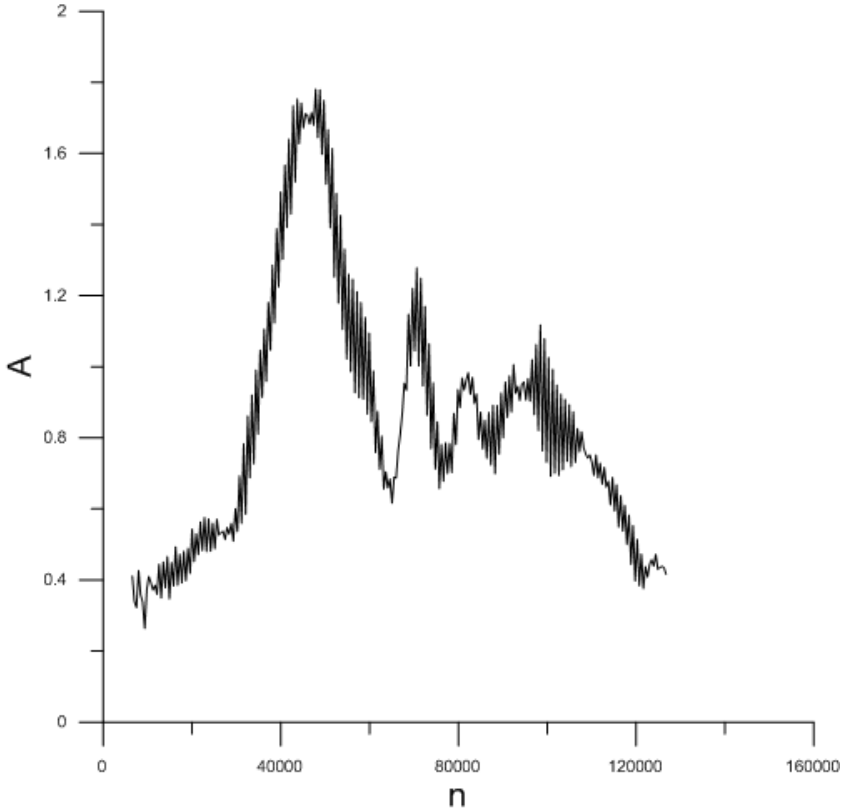

Fig. 4.13. The dependence of the signal amplitude angle (by number of reference) for a spherical segment.

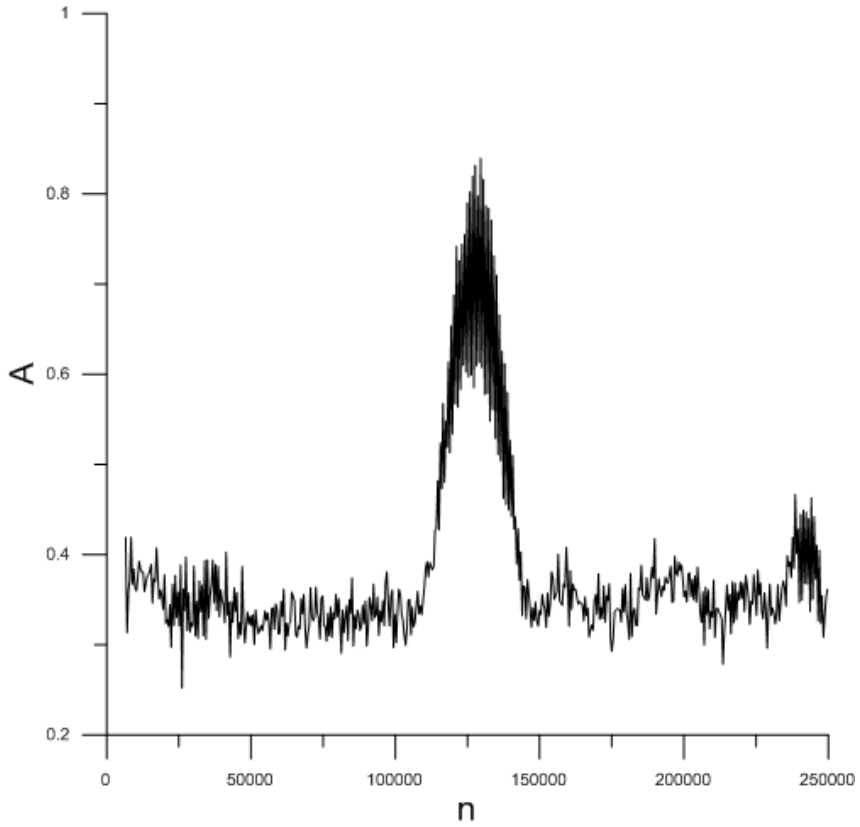

Fig. 4.14. Signal amplitude dependence on the angle of rotation (by number of reference) for the cylinder.

Starting values on the graph corresponds to the position of the cylinder when it is perpendicular to the axis of symmetry of the incident wave. The length of the cylinders is 4.95λ and diameter is 1.98 λ.

Starting values on the chart for a spherical segment corresponds to the position where the symmetry axis is rejected by 45 degrees from the axis of the incident wave. Radius of the sphere and the underlying segment of a sphere is 4.95λ.

From samples number it is easily to go to degrees, knowing how big turn the body made during the observation, given that the second recorded 1 000 samples.

For example, for a cylinder, which made a turnover of 180 degrees for 250 seconds, the schedule will be as follows:

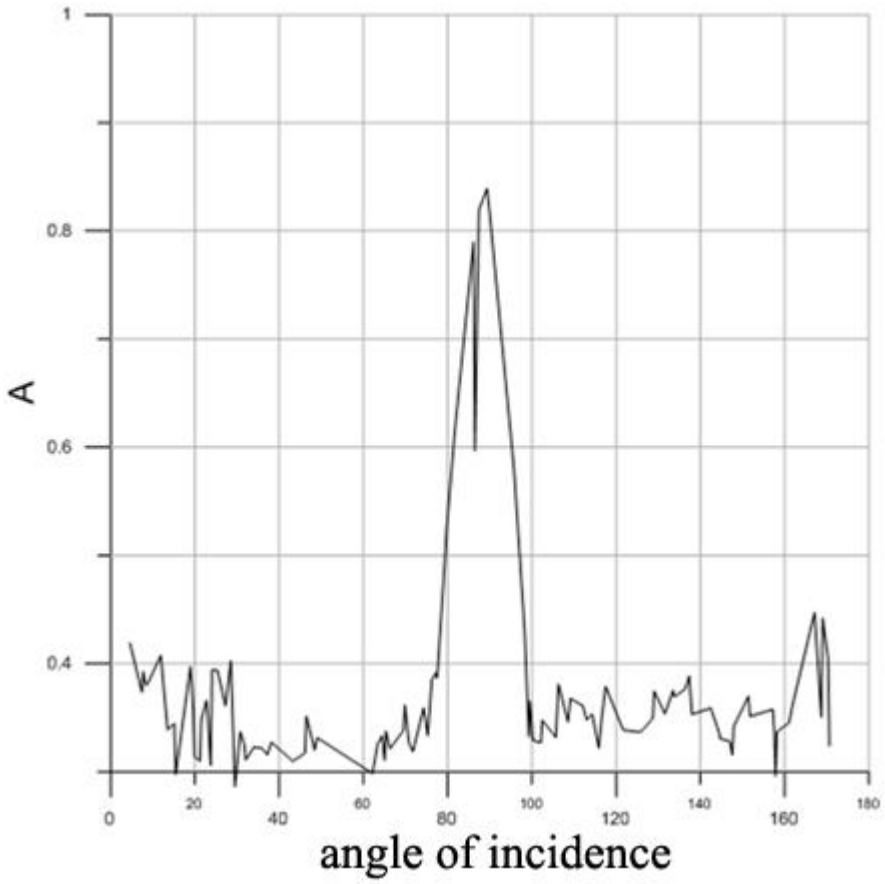

Fig. 4.15 The dependence of the signal amplitude on the rotation angle for the cylinder.

So, using the calibration curves shown in Fig. 4.6-4.7, as well as calculating the theoretical value of the formulas of the RCS at the maximum, one can obtain dimensionless units of amplitude per unit area.

For example, the maximum RCS for a corner reflector is calculated as: $\sigma_{max} = \frac{8\pi w^2 h^2}{\lambda^2}$, where w is the width and h is the height of a rectangular plate (plates, forming an angle, should be equal). Then for the measured angle reflector, the maximum on the graph corresponds to a value of 9.77 m^2. The corresponding formulas for the maximum value of the RCS depending on the size of the object:

For the sphere: $\sigma_{max} = \pi * R^2$

for a circular cylinder $\sigma_{max} = \frac{2\pi r h^2}{\lambda}$.

It should be noted that other method can be used instead the VLF signal filtering method and the synchronous detection method. That is matched filtering. To select the FM signal it is necessary to synchronize the movement of the mechanism. To do this, the mechanism must be equipped with motion sensors to track the position of the slider or give readings when the slider is in the extreme positions. This upgrade was not available, so this method has not been implemented.

4.4. Comparison with previously published data

Due to the fact that the sizes of the objects for which theoretical values of RCS were calculated, as well as the experimental values were found, have different dimensions from sizes studied in this paper, objects, graphics of RCS can be compared only qualitatively.

By comparing results with data from the literature [7] we see that for the dihedral corner reflector we obtained more conspicuous at least after passing through a maximum, the overall behavior is the same.

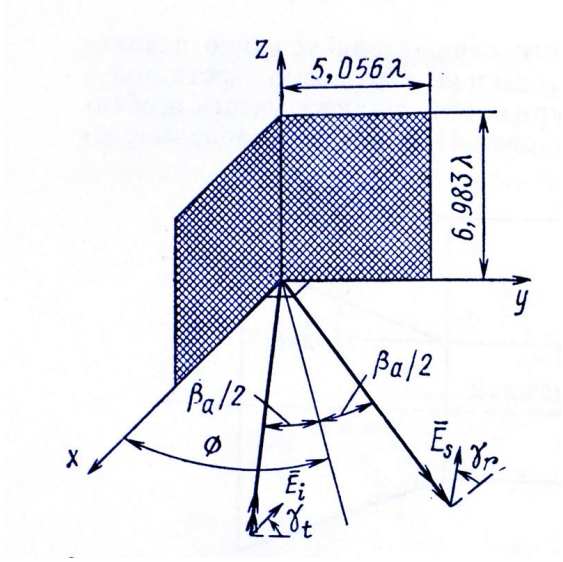

Fig. 4.16 dihedral corner reflector.

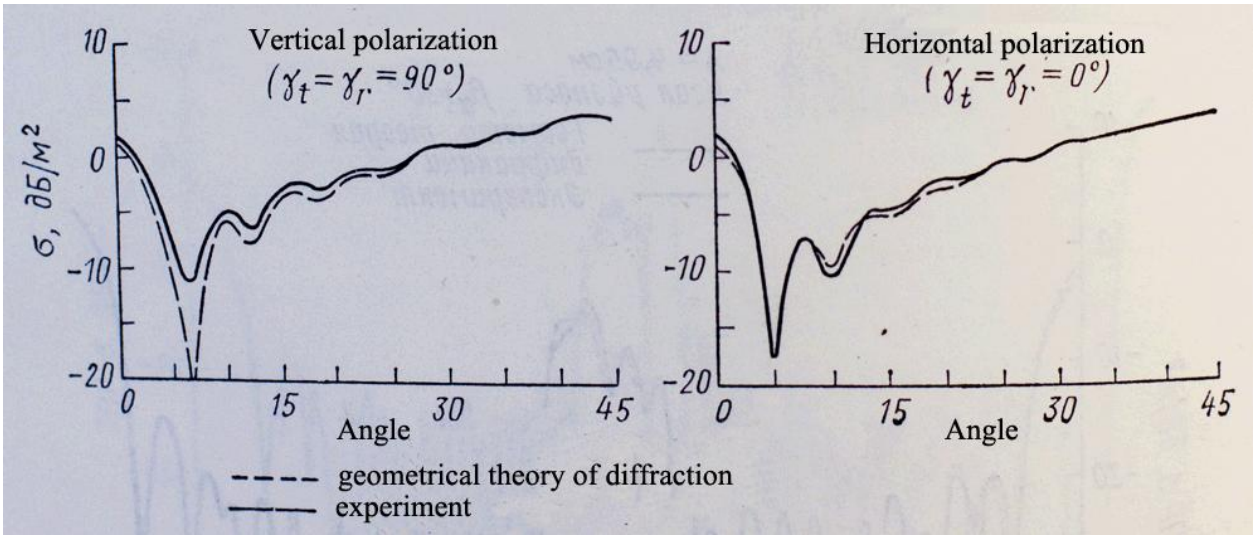

Fig. 4.17 RCS of a dihedral corner reflector for monostatic radar

RCS for a circular cylinder also has the same peaks as calculated experimentally in [7]. Maximum corresponding to the rotation 90^0 and Fig.4.18 exceeds the maximum for a turn in 0^0, which is also present on the experiment data Fig.4.14and 4.15.

Theoretical data on the segment of a sphere was not found, but the dependence on Fig.4.13 coincides with the theoretical curve for the sphere on the site 0-65000 counts. The subsequent behavior of the RCS depending on the angle most likely is due to defects in the manufacturing segment of a sphere and the roughness of its surface, which causes additional reflections.

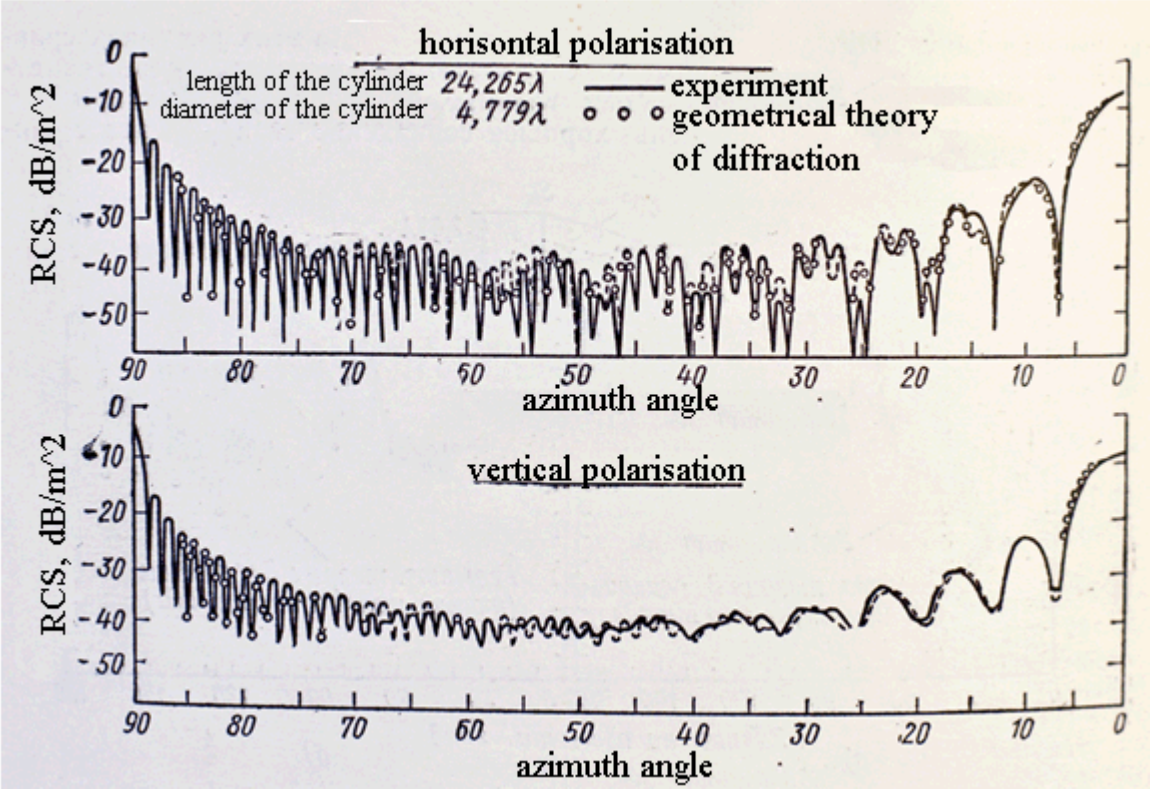

Fig. 4.18 RCS of a circular cylinder for vertical and horizontal polarization.

Conclusion

The installation allows to make measurements in the range of 200,000: 1 (estimated from the ratio of the amplitude of the maximum of the measured signal to the amplitude of the noise signal). Two methods of signal processing of microwave detectors were investigated - filtering narrowband ULF, synchronous detection. The technique of implementing synchronous detection with quadrature channels was developed. RCS charts for a number of lenses were measured: a spherical segment, corner reflector and a circular cylinder. RCS of horn antenna transceivers was measured and the estimation of the distribution of the field of the measured object was made.

References

1. E.Maizels V.Torgovanov Измерение характеристик рассеяния радиолокационных целей / Советское радио, Москва, 1972.
2. V.P. Akimov, O.B.Utrobin, D.V.Shannikov Изучение и распространение электромагнитных волн Лабораторный практикум / Санкт-Петербург 1991.
3. Отражательная способность радиолокационных целей / Труды института инженеров по электронике и радиоэлектронике / Processing of the IEEE, 1965
4. Распространение ультракоротких волн / «Советское радио», 1954
5. Кинг Р., У Тай-Цзунь. Рассеяние и дифракция электромагнитных волн. / Изд-во иностранной литературы, 1961.
6. User Guide and Specifications NI 6008/6009 / National Instruments
7. M.Skolnik Справочник по радиолокации. / Советское радио, Москва, 1976
8. M.I. Finkelshtein Основы радиолокации. Учеб. для вузов. 2-е изд. / М.: Радио и связь, 1983.
9. J.R.Mezner Дифракция и рассеяние радиоволн / Советское радио, Москва ,1958
10. Jeffrey Travis. LabView for everyone
11. P.V.Makovetsky V.G.Vasiliev Отражение радиолокационных сигналов Лекции / Ленинград 1975
12. Scharfman H. and King D. D. Antenna scattering measurements by modulation of the Scatter. / Proc. IRE, 1954, v. 42, № 5.
13. O.N.Rusak, K.R.Malayan «Безопасность жизнедеятельности» / Издательство «Лань», Санкт-Петербург
14. E.F.Knott, J.F.Shaeffer, M.T.Tuley Radar Cross Section Second Edition / SciTech Publishing, 2004